

1 **Convergent utilization of APN receptor by hedgehog merbecoviruses**

2 Peng Liu<sup>1,7</sup>, Qianhui Zhu<sup>2,3,7</sup>, Jingyi Liu<sup>4,7</sup>, Zhixing Ma<sup>1,7</sup>, Yuanling Yu<sup>5</sup>, Chen Liu<sup>1</sup>, Chengbao Ma<sup>1</sup>,  
3 Junyu Si<sup>1</sup>, Xiao Yang<sup>1</sup>, Meiling Huang<sup>1</sup>, Yehui Sun<sup>1</sup>, Xiao Yu<sup>1</sup>, Yucheng Sun<sup>1</sup>, Tianci Liu<sup>2,3</sup>,  
4 Lingling Yu<sup>5</sup>, Qianran Wang<sup>5</sup>, Jing Li<sup>1</sup>, Yunlong Cao<sup>4,5,6,\*</sup>, Xiangxi Wang<sup>2,3,\*</sup>, Huan Yan<sup>1,8,\*</sup>

5  
6 **Affiliations:**

7 <sup>1</sup>State Key Laboratory of Virology and Biosafety, Hubei Provincial Research Center for Basic  
8 Biological Sciences, College of Life Sciences, TaiKang Center for Life and Medical Sciences,  
9 Wuhan University; Wuhan, Hubei, China

10 <sup>2</sup>Key Laboratory of Biomacromolecules (CAS), National Laboratory of Biomacromolecules, CAS  
11 Center for Excellence in Biomacromolecules, Institute of Biophysics, Chinese Academy of  
12 Sciences, Beijing, China

13 <sup>3</sup>University of Chinese Academy of Sciences, Beijing, China

14 <sup>4</sup>Biomedical Pioneering Innovation Center (BIOPIIC), Peking University, Beijing, China

15 <sup>5</sup>Changping Laboratory, Beijing, China

16 <sup>6</sup>Peking-Tsinghua Center for Life Sciences, Tsinghua University, Beijing, China

17 <sup>7</sup>These authors contributed equally to this work.

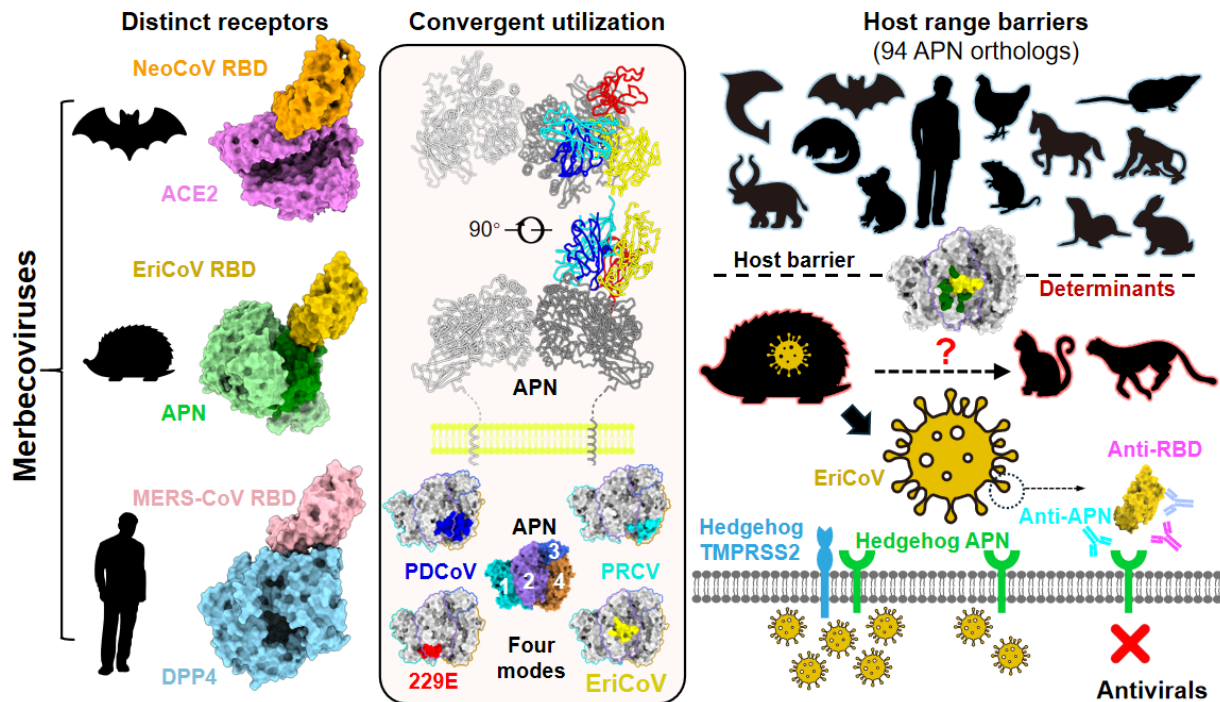
18 <sup>8</sup>Lead contact

19  
20 \*Correspondence: Yunlong Cao: [yunlongcao@pku.edu.cn](mailto:yunlongcao@pku.edu.cn) (Y.C.), Xiangxi Wang:  
21 [xiangxi@ibp.ac.cn](mailto:xiangxi@ibp.ac.cn) (X.W.), Huan Yan: [huanyan@whu.edu.cn](mailto:huanyan@whu.edu.cn) (H.Y.)  
22

## SUMMARY

Dipeptidyl peptidase-4 (DPP4) and angiotensin-converting enzyme 2 (ACE2) are well-established receptors for merbecoviruses, yet the receptor usage of merbecoviruses of European and Asian hedgehogs (EriCoVs) remains unknown. Here, by testing hedgehog orthologs of known coronavirus receptors, we identify hedgehog aminopeptidase N (APN) as a functional receptor for EriCoVs. Analysis of 94 APN orthologs indicates that EriCoVs have a limited host range, primarily utilizing hedgehog APN and, to a lesser extent, APN from certain felids, shaped by specific determinants at the virus–receptor interface. Cryo-EM reveals an APN-binding mode distinct from those used by alpha- and deltacoronaviruses. Functional assays indicate that hedgehog transmembrane serine protease 2 (TMPRSS2) enhances spike activation and promotes pseudovirus entry. Neutralizing antibodies targeting RBD and APN were developed and could effectively block EriCoV pseudovirus entry and propagation. These findings reveal an unexpected convergent evolution of APN utilization among merbecovirus, establishing a foundation for risk assessment and countermeasure development.

**Keywords:** *Merbecovirus*; EriCoV; APN; receptor; hedgehog; TMPRSS2; Neutralizing antibodies



**Graphic abstract:** Convergent utilization of hedgehog APN by EriCoVs

## 1 INTRODUCTION

2 Three human betacoronaviruses—SARS-CoV-1, MERS-CoV, and SARS-CoV-2—have caused  
3 devastating outbreaks in the 21<sup>st</sup> century.<sup>1–5</sup> Among betacoronaviruses, the *Merbecovirus*  
4 subgenus has been designated a priority pathogen group by the World Health Organization  
5 (WHO).<sup>6,7</sup> These viruses include the highly pathogenic Middle East respiratory syndrome  
6 coronavirus (MERS-CoV), which infects both humans and camels,<sup>3,8,9</sup> along with numerous  
7 relatives with varying degrees of zoonotic potential.<sup>10–12</sup>

8  
9 Among them, *Betacoronavirus cameli* (MERSr-CoV), *Betacoronavirus pipistrelli* (HKU5), and  
10 *Betacoronavirus tytonycteridis* (HKU4) are three viral species that originated in bats<sup>13–18</sup> and have  
11 spilled over into mammals such as humans,<sup>3</sup> camels,<sup>19–21</sup> pangolins,<sup>22,23</sup> and minks.<sup>24</sup> In 2013, a  
12 novel merbecovirus species (*Betacoronavirus erinacei*, or EriCoV/ErinCoV) was discovered in  
13 fecal samples from European hedgehogs (*Erinaceus europaeus*, *E.eur*) in Germany.<sup>25</sup> A related  
14 Asian lineage (HKU31) was later found in Amur hedgehogs (*Erinaceus amurensis*, *E.amu*) in  
15 China.<sup>26</sup> To date, EriCoVs have been reported exclusively in hedgehogs across a broad  
16 geographic range across Euroasia, including Germany,<sup>25</sup> France,<sup>27</sup> United Kingdom,<sup>28</sup> Italy,<sup>29,30</sup>  
17 Poland,<sup>31,32</sup> Portugal,<sup>33</sup> Russia,<sup>34</sup> and China.<sup>26,35,36</sup> Among them, all Asian EriCoVs were sampled  
18 in *E.amu* hedgehogs, while nearly all European EriCoVs were found in *E.eur* hedgehogs, except  
19 for two strains from Moscow annotated as *Erinaceus sp.*<sup>34</sup> Despite their broad geographic  
20 distribution and genetic diversity, EriCoVs remain poorly understood in terms of pathogenicity and  
21 cross-species potential.<sup>27,33</sup>

22  
23 The host range and transmissibility of coronaviruses are primarily determined by interactions  
24 between the spike (S) protein receptor-binding domain (RBD) and specific cellular receptors.<sup>37</sup> So  
25 far, at least five host proteins have been established as functional coronavirus receptors:  
26 carcinoembryonic antigen-related cell adhesion molecule 1a (CEACAM1a),<sup>38,39</sup> angiotensin-  
27 converting enzyme 2 (ACE2),<sup>40–42</sup> dipeptidyl peptidase-4 (DPP4),<sup>14,15,43</sup> aminopeptidase N  
28 (APN),<sup>44,45</sup> and transmembrane protease serine 2 (TMPRSS2).<sup>46–49</sup> Among them, ACE2 and APN  
29 are recognized by phylogenetically diverse coronaviruses with distinct RBD structures, indicating  
30 multiple independent receptor acquisition events during evolution.<sup>50–52</sup> ACE2 usage is shared by  
31 coronaviruses across alpha- and betacoronavirus, including setracoviruses (e.g., NL63<sup>41</sup>),  
32 sarbecoviruses (e.g., SARS-CoV-2<sup>5,53,54</sup>), and several merbecovirus clades (e.g., NeoCoV,<sup>40</sup>  
33 MOW15-22,<sup>51</sup> HKU5,<sup>24,50,55–57</sup> HKU25<sup>58</sup>). APN serves as a receptor for multiple alpha- and  
34 deltacoronaviruses, including duvinacoviruses (e.g., 229E<sup>44</sup>), tegacoviruses (e.g., TGEV,<sup>45</sup>  
35 CCoV-HuPn-2018,<sup>59</sup> FCoV-23<sup>60</sup>), and buldecoviruses (e.g., PDCoV,<sup>61</sup> and multiple Avian  
36 deltacoronaviruses<sup>62</sup>). TMPRSS2, besides serving as a functional receptor for HKU1, is also a  
37 critical protease for spike activation of many coronaviruses, influencing the route and tropism of  
38 these viruses.<sup>54,63–65</sup>

39  
40 While DPP4 has been considered the canonical receptor for merbecoviruses, recent findings  
41 suggest that ACE2 may be more prevalent than previously apprehended.<sup>40,50,51,57</sup> In 2022, we  
42 reported that NeoCoV and PDF-2180, close relatives of MERS-CoV in African bats, use ACE2  
43 as their functional receptors.<sup>40,66</sup> Subsequently, several other merbecovirus clades were also  
44 found to acquire ACE2 usage independently.<sup>50,51,57,58</sup> However, EriCoVs do not use either ACE2  
45 or DPP4 for entry, leaving their entry and transmission mechanism unresolved.<sup>40,56,67</sup>

1  
2 Here, we show that EriCoVs use hedgehog APN as an entry receptor and rely on hedgehog  
3 TMPRSS2 for spike activation. Cryo-EM analyses unveil a previously unrecognized APN-binding  
4 mode, representing another unique case of convergent APN utilization by betacoronavirus. This  
5 study provided the last major piece to the long-standing puzzle of merbecovirus receptor usage,  
6 and points the way toward effective assessment and mitigation of the zoonotic threats posed by  
7 those MERS-CoV relatives.

8  
9

## 1 RESULTS

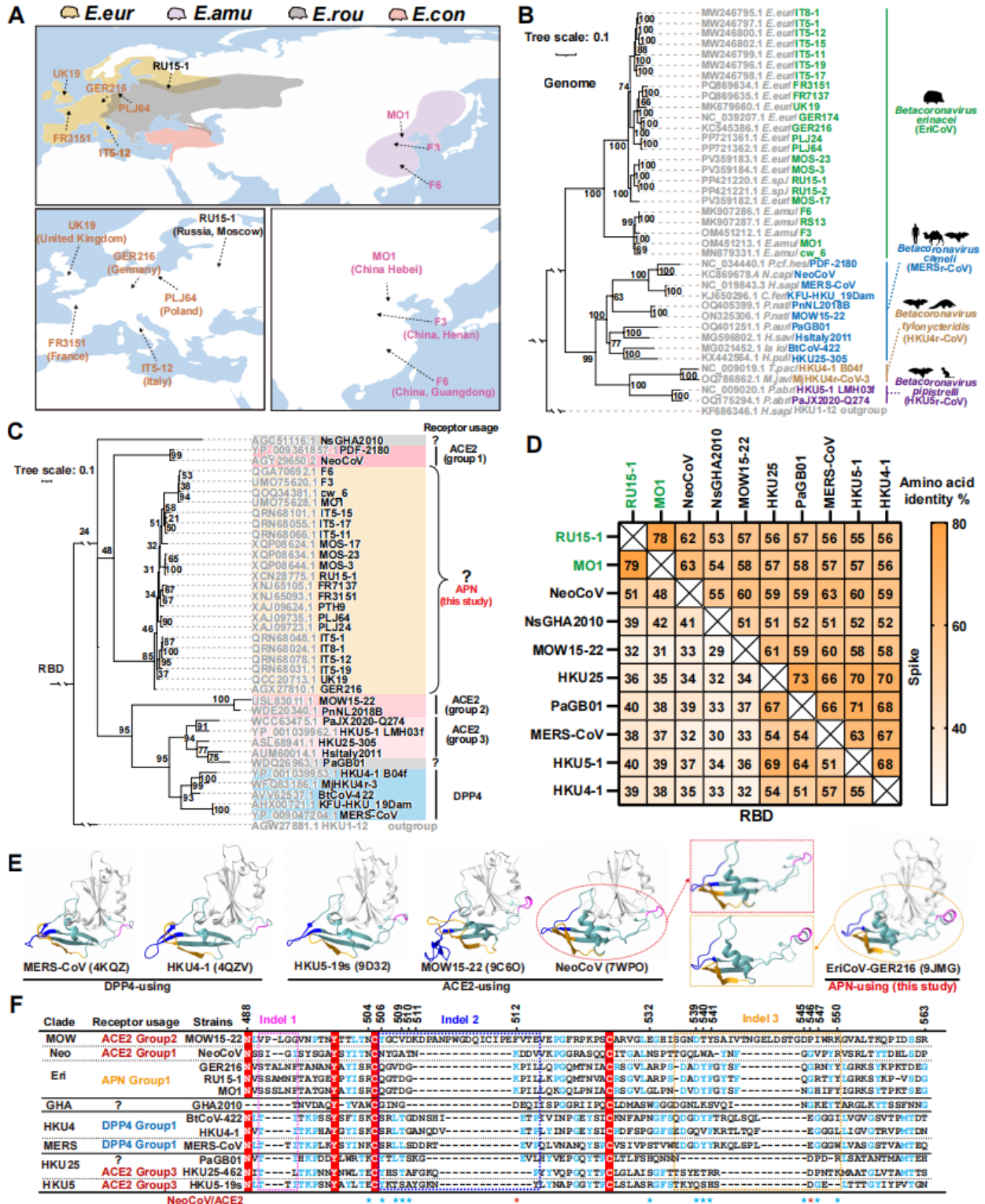
### 3 Characterization of EriCoV receptor binding domain

4 To investigate the receptor binding features of EriCoVs, we analyzed 24 publicly available EriCoV  
5 genomic sequences and 25 EriCoV S glycoprotein sequences, with particular focus on the RBD  
6 regions. For conciseness and clarity, EriCoV strain names were abbreviated in this study ([Figure](#)  
7 [S1A](#) and [Data S1](#)). Among these, 5 Asian EriCoV strains (HKU31) were identified in Amur  
8 hedgehogs (*E. amurensis*) from several provinces of China, while 20 European EriCoV strains  
9 were identified in various European countries, predominantly confirmed from European  
10 hedgehogs (*E. europaeus*) ([Figure 1A](#)).

11  
12 Phylogenetic analyses of both genomic sequences and S glycoprotein amino acid sequences  
13 revealed that Asian and European EriCoVs form sister lineages, distant from bat-borne  
14 merbecoviruses ([Figures 1B](#) and [S1B](#)). This separation suggests a long-term evolutionary  
15 divergence of EriCoVs in hedgehogs across Eurasia. Consistent with previous findings, EriCoV  
16 RBD sequences cluster with those of ACE2-using NeoCoV and PDF-2180, implying a potential  
17 shared ancestry ([Figure 1C](#)).<sup>40</sup> However, due to limited sequence homology and likely different  
18 receptor usage patterns, we classified EriCoVs and NeoCoV-related viruses into distinct clades  
19 in this study. Among the analyzed sequences, pairwise amino acid sequence analysis of S and  
20 RBD shows that two representative EriCoV strains from Asian and European, respectively, share  
21 moderate sequence identity (78~79%), but both are markedly divergent from other  
22 merbecoviruses (32~51% for RBD and 53~63% for S), with NeoCoV being the closest known  
23 strain ([Figure 1D](#)).

24  
25 Structural comparison of RBDs from representative merbecoviruses revealed that EriCoV and  
26 NeoCoV share a similar overall RBD core and receptor-binding motif (RBM) architecture,  
27 including characteristic insertion–deletion (indel) patterns ([Figure 1E](#)), which have been  
28 implicated in receptor usage shifts during coronavirus evolution.<sup>58,68</sup> Further examination of the  
29 putative RBM sequences confirmed shared indel patterns between NeoCoV and EriCoVs, except  
30 for indel 1, which lies outside the canonical interaction interface. However, only 2 out of 14 ACE2-  
31 interacting NeoCoV residues are conserved in EriCoV,<sup>40</sup> suggesting a distinct receptor  
32 engagement mechanism ([Figure 1F](#)).

33  
34 Collectively, these analyses suggest that EriCoVs likely employ a novel receptor-binding strategy  
35 that does not involve known ACE2 or DPP4 interaction modes, concurring with the observations  
36 in prior studies.<sup>40,56</sup>



1 **Figure 1 | Geographic distribution, phylogenetic relationship, and RBD features of EriCoVs.**  
2 (A) Geographic distribution of Erinaceus hedgehogs and reported sampling locations of selective  
3 EriCoV strains. Host abbreviations: *E.eur* (*Erinaceus europaeus*), *E.amu* (*Erinaceus amurensis*),  
4 *E.rou* (*Erinaceus roumanicus*), *E.con* (*Erinaceus concolor*). Species distribution data retrieved  
5 from the International Union for Conservation of Nature (IUCN) Red List were mapped using  
6 GeoScene Pro. The color scheme of EriCoVs corresponds to their host, except for RU15-1 with  
7 an unconfirmed hedgehog species (*Erinaceus sp.*). (B-C) Maximum-likelihood phylogenetic trees  
8 of representative merbecoviruses based on complete genome nucleotide sequences (B) or RBD  
9 amino acid sequences (corresponding to NeoCoV residues 380–585) (C) were generated by IQ-  
10 TREE. HKU1-12 was designated as the outgroup. Host, viral species, receptor usage, and  
11 receptor binding mode are annotated. ACE2-using merbecoviruses were grouped according to  
12 evolutionarily distinct receptor-binding modes characteristic of the NeoCoV- (clade 1), MOW15-  
13 22- (clade 2), and HKU5/HKU25-related (clade 3) clades. Scale bars denote genetic distance  
14 (substitutions per site). (D) Pairwise amino acid identity matrix of receptor-binding domains (RBDs)  
15 and full-length S glycoproteins for selected merbecoviruses. EriCoV strains were labeled in green.  
16 (E) Structures of representative merbecovirus RBDs. The conserved RBD core subdomains are  
17 rendered in gray, and receptor-binding motifs (RBMs) are rendered in dusty teal; structurally  
18 divergent RBM indels are highlighted (magenta: indel 1; dark blue: indel 2; orange: indel 3). The  
19 magnified RBMs from NeoCoV and EriCoV (GER216) were shown to facilitate comparison. (F)  
20 Manually adjusted multiple sequence alignment of RBMs with optimized indel positioning. Fully  
21 conserved residues are shown with a red background; partially conserved residues are colored  
22 with light blue. Dashed boxes define indels that correspond with panel E. Residues mediating  
23 ACE2 interactions by NeoCoV are asterisked (red: conserved in EriCoVs; blue: divergent).  
24 NeoCoV residue numbering is shown.  
25 See also Figure S1.

26  
27  
28

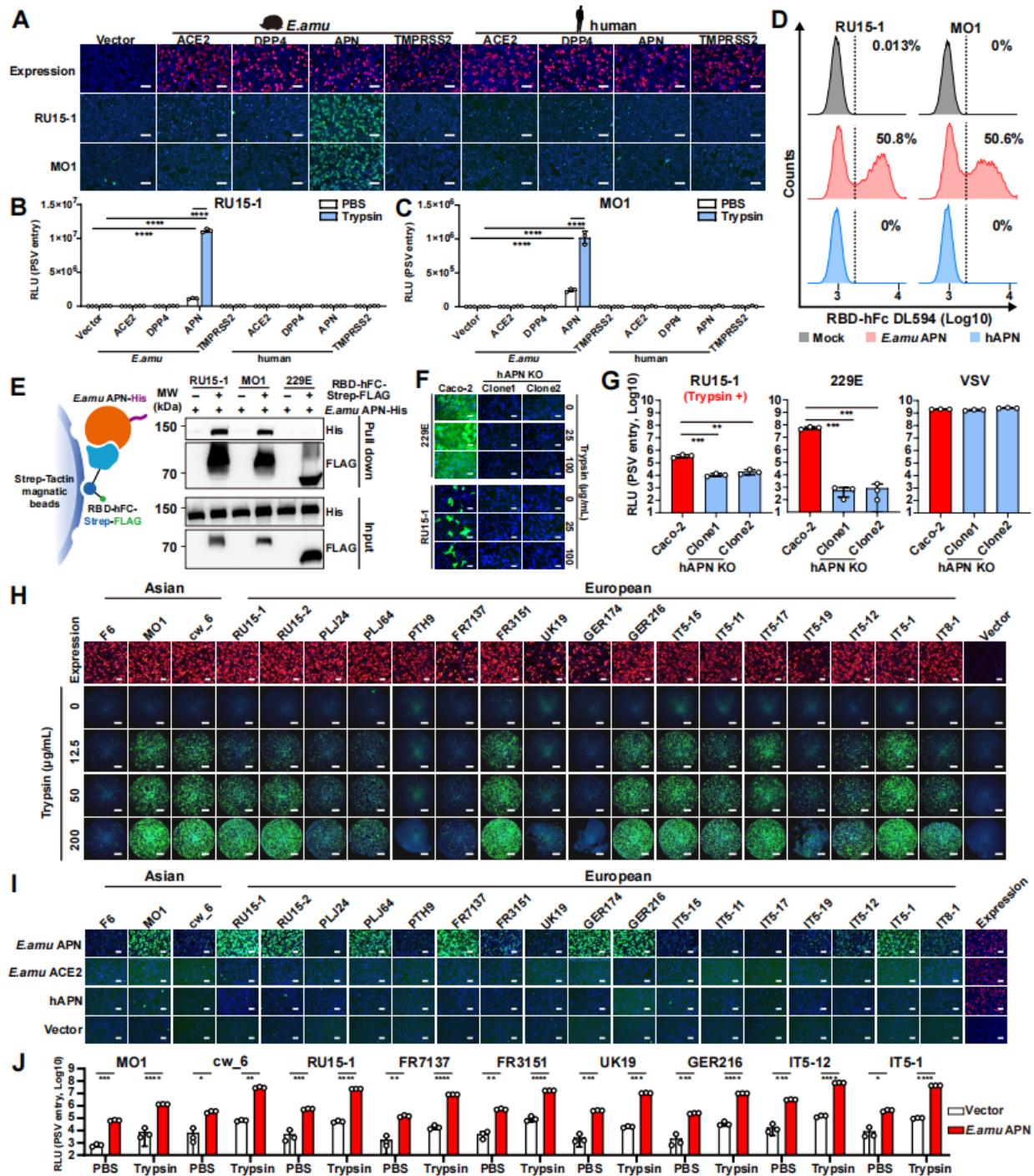
## 1 **Hedgehog APN is a receptor for EriCoV**

2 Given previous failed attempts to identify receptor functionality among various mammalian ACE2  
3 orthologs<sup>40</sup> and the hypothesis that EriCoVs may utilize an uncharacterized receptor binding  
4 mode, we explored whether these viruses engage alternative known coronavirus receptors from  
5 hedgehog hosts, including DPP4, APN, and the recently identified HKU1 receptor TMPRSS2. To  
6 this end, we retrieved protein-coding sequences of ACE2, DPP4, TMPRSS2, and APN from the  
7 RNA-seq data of *E. amurensis* hedgehog (Genome Sequence Archive, GSA database)<sup>69</sup> for  
8 subsequent evaluation. Notably, APN amino acid sequences were identical between *E.amu* and  
9 *E.eur* hedgehogs, allowing *E.amu* APN to serve as a representative for both hedgehog host  
10 species ([Data S2](#)).

11  
12 We first tested two representative EriCoV strains: RU15-1 (European) and MO1 (Asian). Among  
13 the tested receptors, only *E.amu* APN, but not *E.amu* ACE2, DPP4, TMPRSS2, or human (h)  
14 counterparts, supported detectable RBD binding ([Figure 2A](#)) and RU15-1 and MO1 pseudovirus  
15 entry ([Figures 2B and 2C](#)). Flow cytometry confirmed specific binding of EriCoV RBDs to *E.amu*  
16 APN but not to hAPN ([Figure 2D](#)). A pull-down assay further demonstrated that EriCoV RBD, but  
17 not 229E RBD, interacted specifically with *E.amu* APN ([Figure 2E](#)). Notably, mutation of the APN  
18 catalytic site<sup>70</sup> did not impair IT5-12 RBD binding or pseudovirus entry, indicating that receptor  
19 function is independent of protease activity ([Figures S2A and S2B](#)). Although hAPN was not an  
20 efficient receptor for EriCoVs, CRISPR-Cas9 knockout (KO) of endogenously expressed hAPN  
21 abolished the limited EriCoV S-mediated membrane fusion ([Figure 2F](#)) and pseudovirus entry in  
22 Caco-2 cells ([Figure 2G](#)), reducing both to background levels. A similar phenotype was observed  
23 for 229E, which was used as a positive control ([Figure 2G](#)).

24  
25 We next evaluated whether *E.amu* APN also serves as a functional receptor for additional EriCoV  
26 strains. In a cell-cell fusion assay, *E.amu* APN promoted spike-mediated membrane fusion for  
27 most tested strains in a trypsin-dependent manner ([Figures 2H and S2C](#)). Similarly, *E.amu* APN,  
28 but not *E.amu* ACE2 or hAPN, supported S<sub>1</sub>-hFc and RBD-hFc binding from multiple EriCoV  
29 strains to varying efficiencies ([Figure 2I and S2D](#)). These findings were further validated by entry  
30 assays using VSV pseudotyped with S glycoproteins from diverse EriCoV strains ([Figures 2J and](#)  
31 [S2E](#)).

32  
33 Together, these data demonstrate that APN, but not other known coronavirus receptors, serves  
34 as a functional receptor for both Asian and European EriCoVs through specific interaction with  
35 their RBDs.



1  
2 **Figure 2 | Hedgehog APN functions as a receptor for EriCoVs.** (A-C) Transient expression of  
3 *E. amurensis* (*E.amu*) APN, but not *E.amu* ACE2, DPP4, TMPRSS2, nor any tested human  
4 receptor counterparts, supported EriCoV RU15-1 and MO1 RBD human IgG1 Fc domain (hFc)  
5 fusion protein (RBD-hFc) binding (A), as well as pseudovirus entry (B-C) in HEK293T cells.  
6 Receptor expression was confirmed by immunofluorescence staining: FLAG-tagged ACE2, DPP4,  
7 and APN, and ALFA-tagged TMPRSS2 (red). Pseudoviruses (PSV) were pretreated with 1.25  
8 mg/mL trypsin. (D) Flow cytometry analyses of RU15-1 and MO1 RBD-hFc binding to HEK293T  
9 cells transiently expressing hAPN or *E.amu* APN. Dashed lines: background threshold. Means of

1 three technical repeats are shown. (E) Pull-down assay showing specific interaction of soluble  
2 *E.amu* APN ectodomain (His-tagged) with Strep-Tactin-immobilized RU15-1 or MO1 RBD-hFc-  
3 Strep-FLAG fusion proteins, with 229E RBD as a negative control. (F) Cell-cell fusion assays  
4 in Caco-2 or hAPN-knockout (KO) Caco-2 cells (two clones) transiently expressing 229E or RU15-  
5 1 spike proteins, with or without trypsin treatment. (G) Infection of Caco-2 and hAPN-KO Caco-2  
6 cells by the indicated pseudoviruses. RU15-1 pseudoviruses were pretreated with 1.25 mg/mL  
7 trypsin, and infection was performed in serum-free DMEM containing 125 µg/mL trypsin. (H-I) S-  
8 mediated cell-cell membrane fusion (H) and S<sub>1</sub>-hFc binding (I) of indicated Asian and European  
9 EriCoV strains in HEK293T cells stably expressing *E.amu* APN with the treatment of indicated  
10 concentrations of trypsin for panel H, or in HEK293T cells transiently expressing *E.amu* APN,  
11 *E.amu* ACE2, hAPN, or vector control for panel I. S glycoprotein and receptor expression was  
12 evaluated by immunofluorescence, detecting the C-terminally fused HA tag in panel H, and C-  
13 terminally fused FLAG tag in panel I (red). (J) Trypsin-pretreated (1.25 mg/mL trypsin)  
14 pseudovirus entry efficiency of selected EriCoV strains in HEK293T cells transiently expressing  
15 the *E.amu* APN. Mean ± SD and n=3 biological replicates for B, C, G, and J. Statistical significance  
16 was determined using unpaired two-tailed *t* tests. \*\*:  $P < 0.01$ , \*\*\*:  $P < 0.005$ , and \*\*\*\*:  $P < 0.001$ .  
17 RLU: Relative light unit. Scale bars: 100 µm for A, F, I, and 5 mm for H.  
18 See also Figure S2.  
19

## 20 Ortholog specificity and host tropism determinants

21 To assess the potential host range and spillover risk of EriCoVs, we examined the ability of various  
22 APN orthologs to support RBD binding and pseudovirus entry when transiently expressed in  
23 HEK293T cells. We established an APN library comprising 94 orthologs spanning 13 taxonomic  
24 orders (31 bats, 62 non-bat mammalian species, and one avian species), all with validated  
25 expressions (Figures 3A, S3A, and Data S3).  
26

27 Both the European (RU15-1) and Asian (MO1) EriCoV strains bound efficiently to hedgehog APN  
28 (*E.amu* APN) (Figures 3B and S3B). In contrast, APNs from *Sorex araneus* (*S.ara*) and *Suncus*  
29 *etruscus* (*S.etr*), which are also members of the order Eulipotyphla, did not support detectable  
30 binding. Notably, two feline APN orthologs from the leopard (*Panthera pardus*, *P.par*) and  
31 domestic cat (*Felis catus*, *F.cat*) supported detectable RU15-1 and GER216 RBD binding, but not  
32 to MO1, indicating a strain-specific receptor compatibility (Figures 3B and S3B-3C). The receptor  
33 function of *P.par* and *F.cat* APNs was additionally validated across multiple EriCoV strains, and  
34 their ability to promote entry of GER216, FR7137, and PLJ64 highlighted the spillover potential of  
35 selected European EriCoV strains (Figures 3C-3D).  
36

37 To define the molecular basis of this restricted tropism, we constructed domain-swapped  
38 chimeras between human and *E.amu* APNs and assessed their ability to support EriCoV RBD  
39 binding (Figure 3E). Substituting domain 2 of *E.amu* APN with its human counterpart abolished  
40 binding, while substituting *E.amu* Domain 2 with human APN counterpart restored binding,  
41 identifying domain 2 as a key determinant of species specificity. In contrast, swapping domains  
42 1, 3, or 4 had minimal or no effect (Figure 3F). Flow cytometry further confirmed the key  
43 contribution of domain 2 to species specificity (Figure 3G). Fine mapping of domain 2 narrowed  
44 down the key host range determinants within region 288–331 (hAPN numbering), encompassing  
45 β16, β17, α1, and α2. Among them, β16 and α2 are more surface exposed, and the latter contains

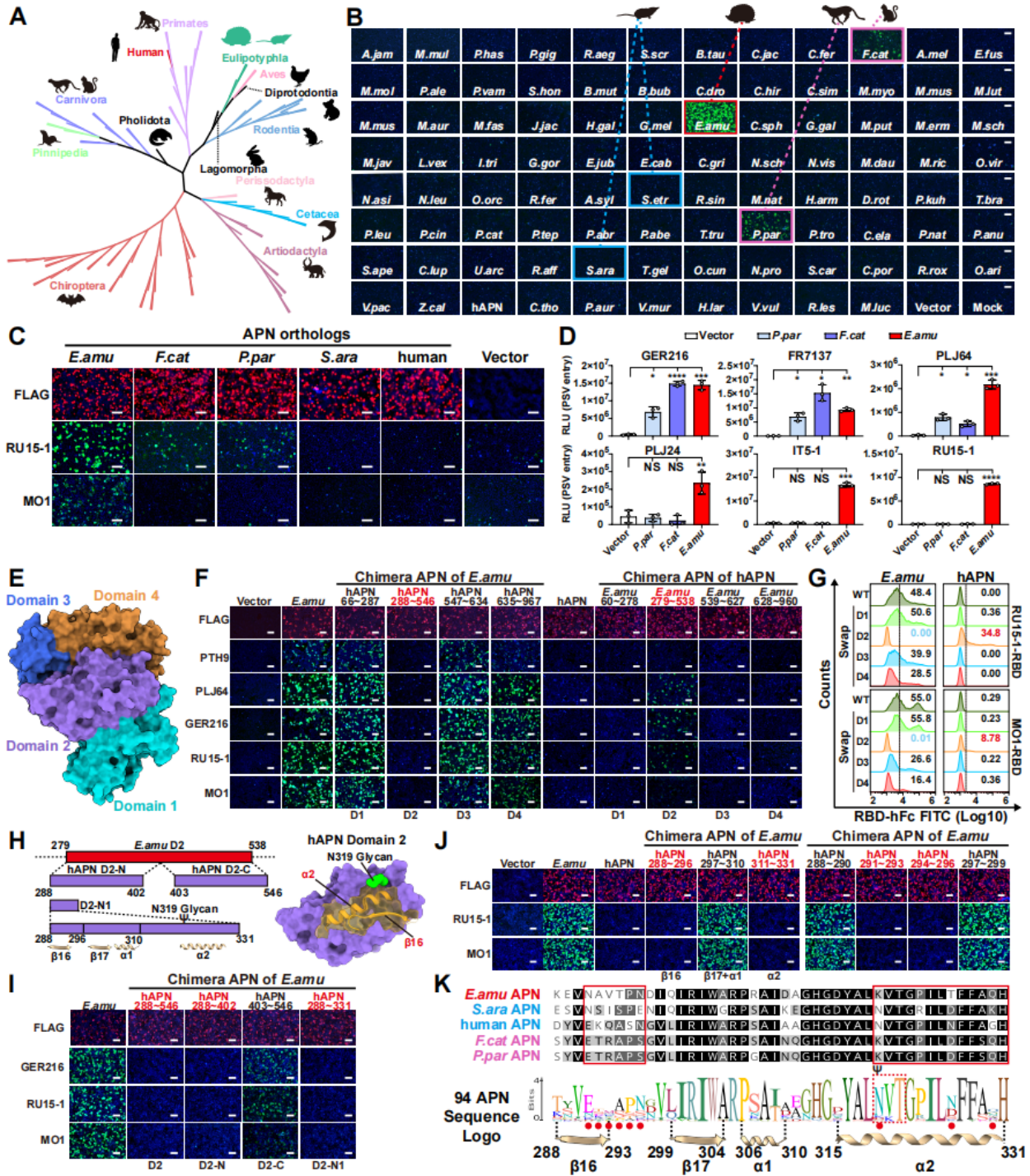
1 an N-319 glycosylation (Figures 3H-3J). Substitution of this region in hAPN with the *E.amu*  
2 counterpart (residues 279–321) enabled RBD binding (Figure S3D). Logoplot analysis based on  
3 the amino acid sequences of the 94 APN orthologs revealed high variability in this region, with  
4 *E.amu* APN displaying unique sequence features, particularly those around  $\beta$ 16, as well as  
5 several key residues in  $\alpha$ 2 (Figure 3K). The partial sequence similarity of this region in *F.cat* and  
6 *P.par* APNs and the absence of an evolutionarily conserved N319-glycosylation, but not in human  
7 or *S.ara* orthologs, likely explains their receptor compatibility.

8

9 Collectively, these findings demonstrate a restricted APN tropism among EriCoVs and suggest  
10 that felids, including domestic cats, may serve as potential spillover hosts. Identification of host  
11 range determinants within the highly variable domain 2 highlights its central role in mediating  
12 EriCoV RBD interaction.

13

14



1  
2 **Figure 3 | Multi-species APN tropism and host range determination of EriCoV.** (A) Maximal  
3 likelihood phylogenetic trees of 94 APN orthologs from mammalian and avian species were  
4 constructed using IQ-TREE based on amino acid sequences. Taxonomic orders were annotated.  
5 Ortholog details are provided in [Data S3](#). (B) Binding of RU15-1 S<sub>1</sub>-hFc (green) to HEK293T cells  
6 transiently expressing the indicated APN orthologs, assessed by immunofluorescence using an  
7 anti-hFc antibody. Red box: efficient binding. Magenta box: detectable binding. Blue box: two  
8 Eulipotyphla species tested with undetected binding. (C) RU15-1 and MO1 RBD-hFc binding  
9 (green) to HEK293T cells transiently expressing the indicated APN orthologs. (D) Entry of

1 selected EriCoV strains into HEK293T cells transiently expressing indicated APN orthologs. PSVs  
2 were pretreated with 1.25 mg/mL trypsin. **(E)** Structural model of human APN with four domains  
3 highlighted in different colors. **(F-G)** Immunofluorescence (F) and flow cytometry (G) analyses of  
4 the indicated EriCoV RBD-hFc binding to HEK293T cells transiently expressing APN chimeras  
5 with domain swaps between human and *E. amu* APNs. Dashed lines: background threshold. Data  
6 shown are the mean of three technical repeats. **(H)** Schematic illustration of *E. amu* APN chimeras  
7 with equivalent residues from hAPN. Secondary structures and their surface localization of  $\beta$ 16  
8 and  $\alpha$ 2 in domain 2 (D2) were illustrated. **(I-J)** Fine mapping of the host range determinant  
9 restricting hAPN binding with RBD-hFc from RU15-1 and MO1. Chimeras exhibiting notable  
10 phenotypic changes are highlighted in red. **(K)** Sequence logo plot displaying the polymorphisms  
11 across APN orthologs. Key secondary structures and critical residues involved in host range  
12 determination were marked with red dots. APN expression (red signal in F, I, and J) was validated  
13 via immunofluorescence targeting the C-terminal FLAG tag. Data are presented as mean  $\pm$  SD  
14 for D. N-319 glycosylation sequon is labeled with  $\Psi$  in panels H and K. Statistical significance was  
15 determined by unpaired two-tailed *t* tests (*n* = 3 biological replicates).\*: *P*<0.05, \*\*: *P*<0.01, \*\*\*:  
16 *P*<0.005, and \*\*\*\*: *P*<0.001, NS: not significant. Scale bars: 100  $\mu$ m for panels B, C, F, J, and I.  
17 See also Figure S3.  
18

## 1 **Structure of *E.amu* APN in complex with RU15-1 RBD**

2 To elucidate the molecular basis underlying *E.amu* APN recognition, we determined the cryo-EM  
3 structure of the RU15-1 RBD in complex with *E.amu* APN. 2D and 3D classification revealed that  
4 RU15-1 RBD binds exclusively to the monomeric form of *E.amu* APN, with no interaction  
5 observed with the dimeric form (Figures 4A and S4A). This observation is consistent with our  
6 results from size-exclusion chromatography and negative-stain electron microscopy (Figures S5A  
7 and S5B). Notably, the RU15-1 RBD–*E.amu* APN complex only accounted for approximately 5%  
8 of the total particles, which is consistent with the relatively low binding affinity and high dissociation  
9 rate of the complex determined by Bio-layer interferometry (BLI) assays (Figure S5C).

10  
11 As expected, structural analysis of purified *E.amu* APN ectodomain proteins revealed that the  
12 monomer adopts two distinct conformations, designated as “closed” and “open” (Figures S4A,  
13 S5D, and S5E), reflecting the structural basis for APN’s multifunctionality.<sup>71</sup> However, cryo-EM  
14 analysis demonstrated that RU15-1 binds exclusively to the “closed” conformation of *E.amu* APN  
15 (Figures 4A and S4A), indicating that RU15-1 binding is conformation-dependent, like PDCoV.<sup>52</sup>  
16 In comparison, HCoV-229E can engage both the “open” and “closed” conformations of human  
17 APN, whereas PRCoV binds only to the “open” conformation of pig APN.<sup>72,73</sup>

18  
19 We also determined the structure of the RU15-1 apo Spike. Cryo-EM analysis revealed that all  
20 RBDs adopt the “down” conformation (Figures S4A and S5F). This conformation is stabilized by  
21 an interaction network formed between glycans and neighboring protein surfaces: the N387  
22 glycan on the RBD forms a hydrogen bond with N255 on the adjacent NTD, the N399 glycan on  
23 the RBD interacts with D527 on a neighboring RBD, and the N159 glycan on the NTD forms a  
24 hydrogen bond with S517 on the adjacent RBD. Collectively, these glycan–protein interactions  
25 lock the apo Spike in the “down” state (Figure S5G). A similar phenomenon has also been  
26 observed in other animal-derived apo spikes within the *Merbecovirus* subgenus, including HKU5,  
27 HKU25, and PDF-2180 (Figure S5H).

28  
29 At the binding interface, the RBM of RU15-1 engages *E.amu* APN primarily through a combination  
30 of hydrophobic and polar interactions. Specifically, RU15-1 RBD residues Y539, Y528, F529, and  
31 A526 collectively form a hydrophobic pocket together with *E.amu* APN residues P314 and F415,  
32 contributing significantly to the binding affinity of the complex. In addition, Y539 and R522 on  
33 RU15-1 RBD form hydrogen bonds with backbone atoms of *E.amu* APN residues K310 and F415,  
34 respectively, thereby reinforcing local binding stability. Furthermore, T537 and D527 of RU15-1  
35 establish additional hydrogen bonds with D306 and Q321 of *E.amu* APN, respectively,  
36 establishing an extensive interaction network that underpins specific recognition of *E.amu* APN  
37 by RU15-1 (Figure 4B).

38  
39 Three distinct APN-binding modes have been reported among coronaviruses. Within the  
40 *Alphacoronavirus* genus, tegacoviruses TGEV, PRCV, CCoV-HuPn-2018, and FCoV-23 share a  
41 common binding mode, while HCoV-229E adopts a different one.<sup>59,60,73–75</sup> The *deltacoronavirus*  
42 PDCoV<sup>52</sup> also utilizes a distinct binding mode, featured by a slightly shifted binding orientation  
43 and footprint compared with tegacoviruses. (Figure 4C and S4B). Our cryo-EM reconstruction  
44 reveals that *betacoronavirus* EriCoV RBD binds to APN in a manner distinct from all previously  
45 known APN-using coronaviruses. Unlike the vertical binding orientations of tegacoviruses and

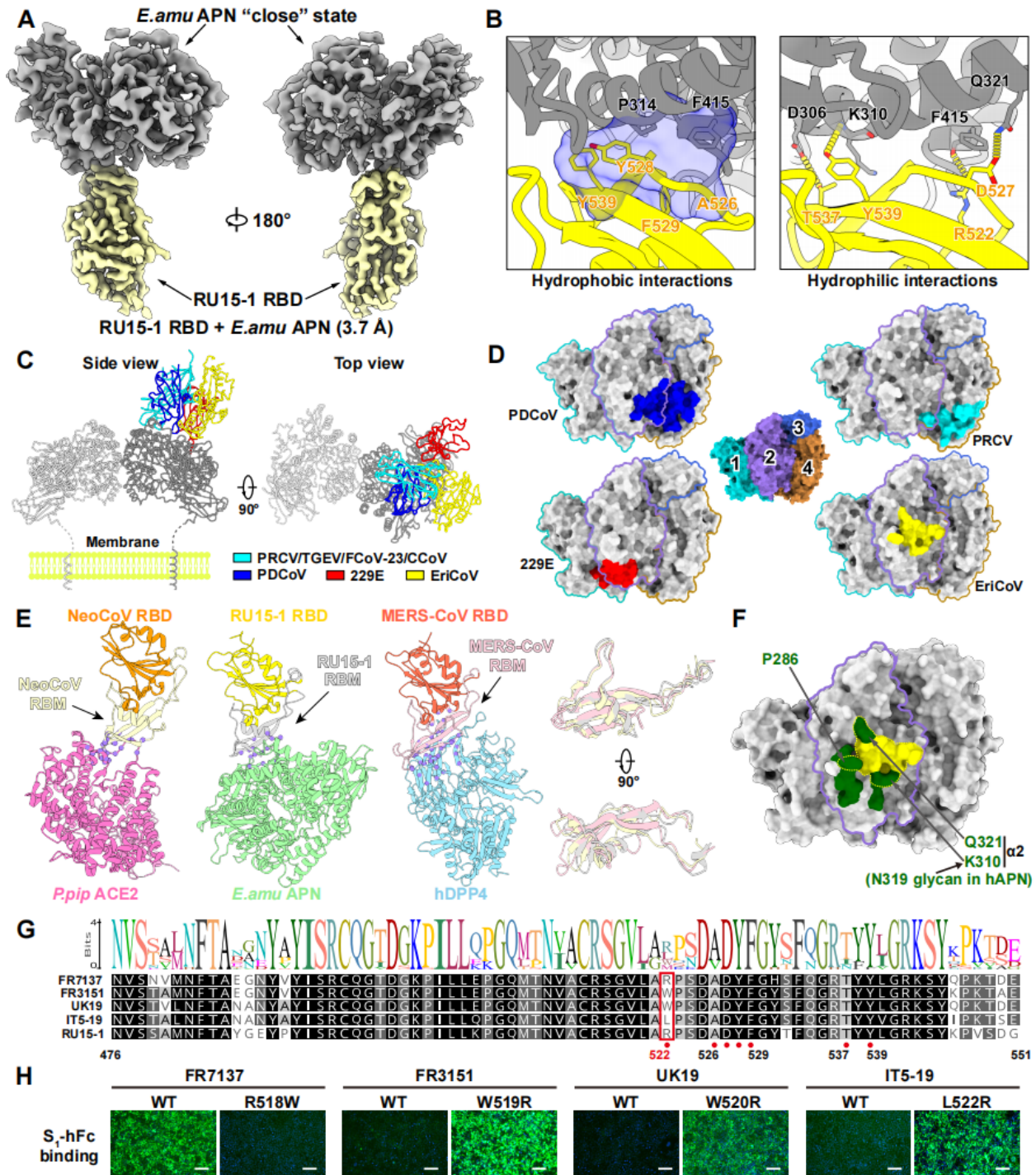
1 PDCoV, or the configuration of 229E, the EriCoV RBD binds APN in a laterally shifted orientation.  
2 Mapping the binding footprints of the four binding modes onto the APN structure showed that  
3 RU15-1 engages a previously uncharacterized region in the central portion of domain 2. Despite  
4 variations, all four RBDs engage domain 2, along with varying contributions from domains 1 and  
5 4 (Figure 4D and S4B). This convergent usage of APN resembles the varying receptor-binding  
6 strategies observed for SARS-CoV-1, SARS-CoV-2, HCoV-NL63, NeoCoV, MOW15-22, and  
7 HKU5, all of which utilize ACE2 as their entry receptor.<sup>40,41,50,51,54,57,76</sup> This EriCoV binding mode  
8 represents a novel mode of APN recognition by merbecoviruses, expanding our understanding of  
9 receptor usage across different coronavirus genera (Figure 4D).

10  
11 Structural comparison of the EriCoV–*E.amu* APN complex with NeoCoV–*P.pip* ACE2 and MERS-  
12 CoV–hDPP4 complexes revealed that all three merbecoviruses utilize the same side of their  
13 RBM—primarily the  $\beta$ -sheet surface—to engage their respective receptors (Figure 4E). However,  
14 distinct indel patterns in the MERS-CoV RBM, as compared with the other two viruses, lead to  
15 conformational remodeling at the RBM tip, driving a shift in receptor specificity. Although EriCoV  
16 shares a similar RBM conformation with NeoCoV, multiple sequence differences at critical contact  
17 sites result in divergent receptor usage.

18  
19 We then examined the molecular mechanisms of receptor species tropism from a structural  
20 perspective. In agreement with our functional data based on human and feline APN orthologs, all  
21 residues identified as critical for host range determination are situated in or around the RU15-1  
22 RBD footprint, with some of them directly contributing to the RBD interaction, such as P286, K310  
23 (corresponding to N319 in hAPN), and Q321 (Figure 4F).

24  
25 To understand the impact of RBM polymorphism on receptor recognition, we generated a  
26 sequence logo plot of 22 EriCoV RBMs. Most residues critical for *E.amu* APN interaction are  
27 highly conserved (Figure 4G). However, the position of R522<sub>RU15-1</sub> displays notable variability,  
28 featuring substitutions with distinct physicochemical properties. To explore the functional  
29 consequences of these variations, we generated several constructs with residue swaps at this  
30 site. Viral antigen binding assay revealed that R at this position confers higher binding affinity to  
31 *E.amu* APN compared to W and L, underscoring the role of EriCoV RBM polymorphism in  
32 modulating receptor binding affinity and probably ortholog specificity (Figure 4H).

33  
34



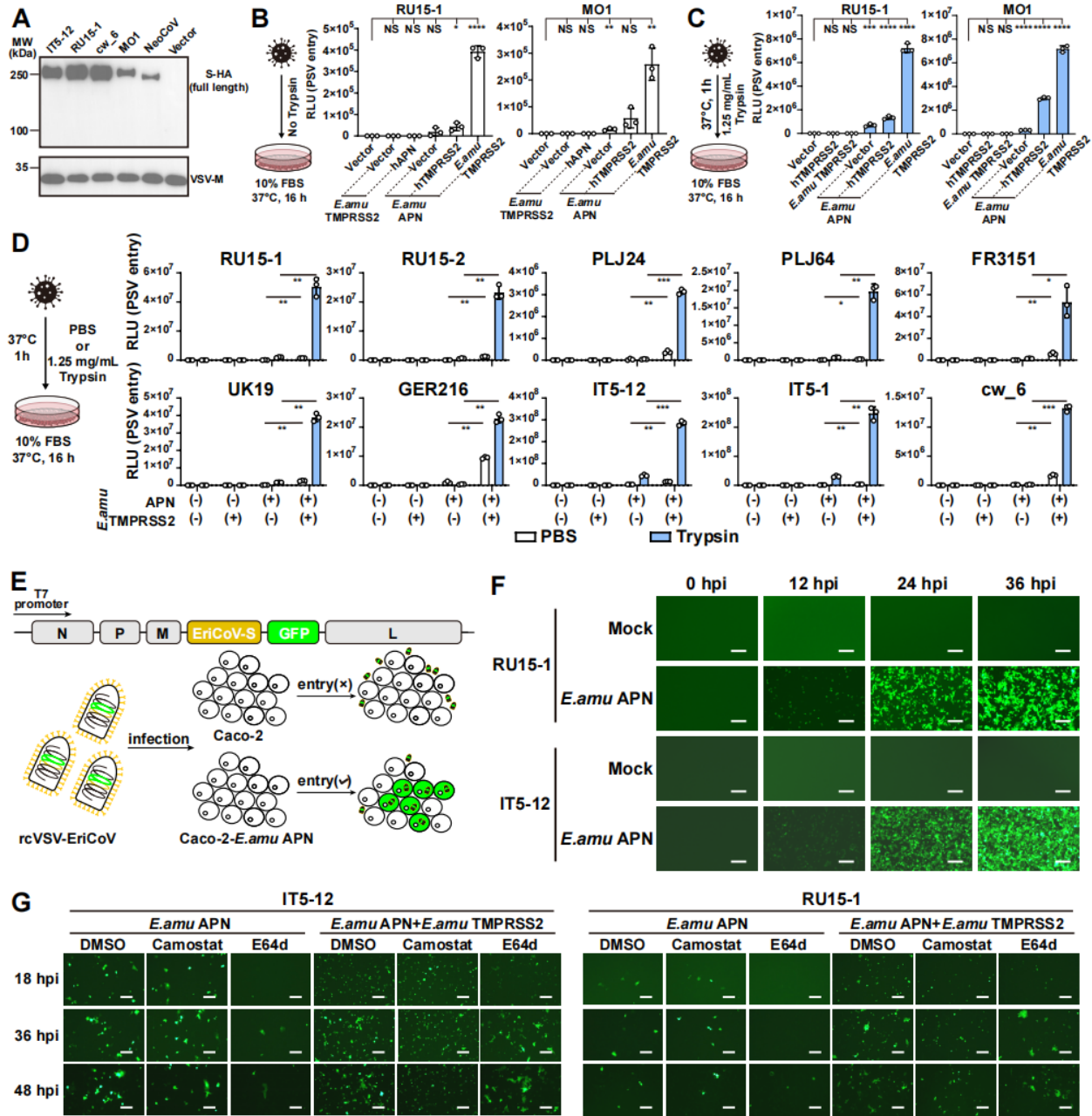
1 common binding mode, and only PRCV is shown as a representative. RBDs of PDCoV (PDB:  
2 7VPP), HCoV-229E (PDB: 8WDE), and EriCoV (RU15-1) (this study) are shown in blue, red, and  
3 yellow, respectively. Only hAPN dimmer is shown for clarity, with individual monomers colored in  
4 silver and gray, respectively. **(D)** RBD footprints of four representative APN-using coronaviruses  
5 mapped onto APN surfaces. APN structures are color-coded: domain 1 in dark turquoise, domain  
6 2 in medium purple, domain 3 in royal blue, and domain 4 in dark goldenrod. RBD footprints follow  
7 the same color scheme as panel C. **(E)** Structural comparison of three merbecovirus binding  
8 modes with distinct receptors: NeoCoV-*P.pip* ACE2 (PDB: 7WPO), EriCoV-*E.amu* APN (PDB:  
9 9W6D) and MERS-CoV-hDPP4 (PDB: 4KR0). Right: Zoomed-in view showing the superimposed  
10 RBMs from each virus. All structures are shown in cartoon representation. The *P.pip* ACE2,  
11 *E.amu* APN, and hDPP4 are colored hot pink, light green, and sky blue, respectively. The RBDs  
12 of NeoCoV, EriCoV, and MERS-CoV are colored dark orange, gold, and tomato, respectively,  
13 with their corresponding RBMs highlighted in wheat, silver, and light pink. **(F)** Summary of the  
14 host range determinants (green) identified in this study and RU15-1 RBD binding interface (yellow  
15 dashed line) mapped onto *E.amu* APN surface. Residue positions in secondary structures are  
16 indicated; domain 2 is outlined in purple. **(G)** Sequence logo plot displaying the polymorphisms in  
17 receptor binding motifs from 22 EriCoV strains. Critical residues involved in APN interaction were  
18 marked with red dots. **(H)** Binding of wild-type and mutant S<sub>1</sub>-hFc proteins from the indicated  
19 European EriCoV strains to HEK293T cells stably expressing *E.amu* APN. Scale bars: 100 μm.  
20 See also Figures S4 and S5.

21  
22 **Hedgehog TMPRSS2-dependent spike activation**  
23 We next examined whether hedgehog APN could promote EriCoV entry and replication in human  
24 cells. As indicated by our earlier pseudovirus entry data (e.g., Figure 2J), EriCoV entry is highly  
25 dependent on trypsin treatment—a method commonly used to facilitate S protein activation via  
26 proteolytic cleavage.<sup>77–79</sup> Analysis of S protein incorporation in selected EriCoV pseudovirus  
27 particles revealed inefficient proteolytic processing during particle biogenesis, similar to what has  
28 been reported for NeoCoV (Figure 5A).<sup>40</sup>

29  
30 To investigate the role of host proteases in EriCoV entry and their cooperation with the receptor,  
31 we first assessed the impact of hTMPRSS2 or *E.amu* TMPRSS2 overexpression on pseudovirus  
32 entry without exogenous trypsin. Under this condition, pseudovirus entry of RU15-1 and MO1 was  
33 undetectable in HEK293T cells unless *E.amu* APN was co-expressed. Although the overall  
34 efficiency is low, entry was markedly increased upon co-expression of *E.amu* TMPRSS2, whereas  
35 hTMPRSS2 weakly enhanced entry, either with or without trypsin treatment (Figures 5B–5C).  
36 Notably, hAPN failed to support detectable entry even in the presence of *E.amu* TMPRSS2,  
37 confirming that hAPN is a poor receptor for EriCoV, and that *E.amu* TMPRSS2 functions in a  
38 receptor-dependent manner.

39  
40 To determine whether this phenotype was specific to RU15-1 and MO1, we evaluated  
41 pseudoviruses of additional EriCoV strains. Since many strains showed lower infectivity, the  
42 pseudoviral particles were pre-treated with trypsin, followed by enzymatic inactivation before and  
43 during infection by 10% FBS. In HEK293T cells transiently expressing the different combinations  
44 of *E.amu* APN and *E.amu* TMPRSS2, all strains displayed similar dependence on APN and  
45 TMPRSS2 co-expression for more efficient entry (Figure 5D).

1  
2 To further assess S-mediated viral propagation, we generated replication-competent VSV (rcVSV)  
3 encoding the S glycoproteins of IT5-12 and RU15-1 ([Figure 5E](#)).<sup>40,50,51</sup> Viral amplification was  
4 observed in Caco-2 cells expressing *E.amu* APN without trypsin treatment ([Figure 5F](#)), but not in  
5 parental Caco-2 cells. In Caco-2 cells overexpressing *E.amu* APN only, rcVSV-RU15-1 and  
6 rcVSV-IT5-12 propagated over time and were sensitive to the cathepsin B/L inhibitor E64d, which  
7 indicates these viruses predominantly adopt the endocytosis pathway under this condition.<sup>54,80</sup>  
8 Cells co-expression of *E.amu* APN and *E.amu* TMPRSS2 supported more efficient rcVSV  
9 amplification, and the boosted infection becomes less sensitive to E64d treatment, while  
10 syncytium formation reduced upon TMPRSS2 inhibitor Camostat treatment,<sup>54</sup> indicating *E.amu*  
11 TMPRSS2 allows more viruses to enter the cell through a cathepsin-independent cell surface  
12 fusion route ([Figure 5G](#)).  
13



1

1 **Figure 5 | EriCoVs rely on hedgehog Tmprss2 for efficient entry and propagation. (A)**  
2 Detection of EriCoV S glycoprotein in VSV pseudovirions via Western blot using an anti-HA  
3 antibody targeting the C-terminally fused HA tag. VSV-M serves as a loading control. **(B-C)** Entry  
4 of RU15-1 and MO1 pseudovirus into HEK293T cells transiently expressing the indicated APN  
5 and Tmprss2 orthologs. Flowcharts summarize the infection conditions with PBS (B) or trypsin  
6 (C) treatment. **(D)** Entry efficiency of selected EriCoV pseudoviruses into HEK293T cells  
7 expressing the *E.amu* APN, *E.amu* Tmprss2, or both. PSVs were pretreated with 1.25 mg/mL  
8 Trypsin, and infection was conducted in the presence of 10% FBS without trypsin. **(E)** Schematic  
9 illustration of the genetic organization and amplification workflow for rcVSV-S constructs encoding  
10 EriCoV S glycoproteins. **(F)** Amplification of rcVSV-RU15-1 and rcVSV-IT5-15 in Caco-2 cells with  
11 or without the expression of *E.amu* APN. **(G)** Propagation of rcVSV-RU15-1 and rcVSV-IT5-12 in  
12 Caco-2 (left) or Caco-2-*E.amu* Tmprss2 (right) cells with the transient expression of *E.amu* APN.  
13 Data are presented as mean  $\pm$  SD for B, C, and D. Statistical significance was determined using  
14 unpaired two-tailed *t* tests (*n* = 3 biological replicates). \*: *P*<0.05, \*\*: *P*<0.01, \*\*\*: *P*<0.005, \*\*\*\*:  
15 *P*<0.001, and NS: not significant. Scale bars: 200  $\mu$ m for panels F and G.  
16

## 1 **Neutralizing antibodies against EriCoV**

2 Next, we investigated whether RBD-targeting antibodies could block viral infection of HEK293T-  
3 *E.amu* APN cells. Mice were immunized with RBD proteins from the MO1 and RU15-1 strains,  
4 which share only 79% identity in their RBD sequences (Figure 6A). ELISA results confirmed that  
5 two immunizations generated specific antibodies against both the MO1 and RU15-1 RBDs,  
6 validating successful immunization (Figure 6B).

7  
8 Based on post-second-immunization ELISA titers, we selected the three highest-titer mice per  
9 group for splenocyte isolation. We sorted single B cells (7-AAD<sup>-</sup>/CD19<sup>+</sup>/IgM<sup>-</sup>/IgD<sup>-</sup>/OVA<sup>-</sup>/RBD<sup>+</sup>)  
10 and expressed monoclonal antibodies from them (Figure S6A). In total, we obtained 54 MO1  
11 RBD-binding antibodies and 67 RU15-1 RBD-binding antibodies (Table S2). We evaluated these  
12 for their ability to neutralize MO1 and RU15-1 pseudoviruses in HEK293T-*E.amu* APN cells, which  
13 revealed potent neutralizing activity for some clones (Figure 6C). Among the 54 MO1-targeting  
14 antibodies, 36 (67%) exhibited strong neutralizing activity (IC<sub>50</sub> < 0.1 µg/mL). In contrast, only 8  
15 (12%) of the RU15-1-targeting antibodies displayed strong neutralizing activity, while 46 (69%)  
16 showed no neutralization.

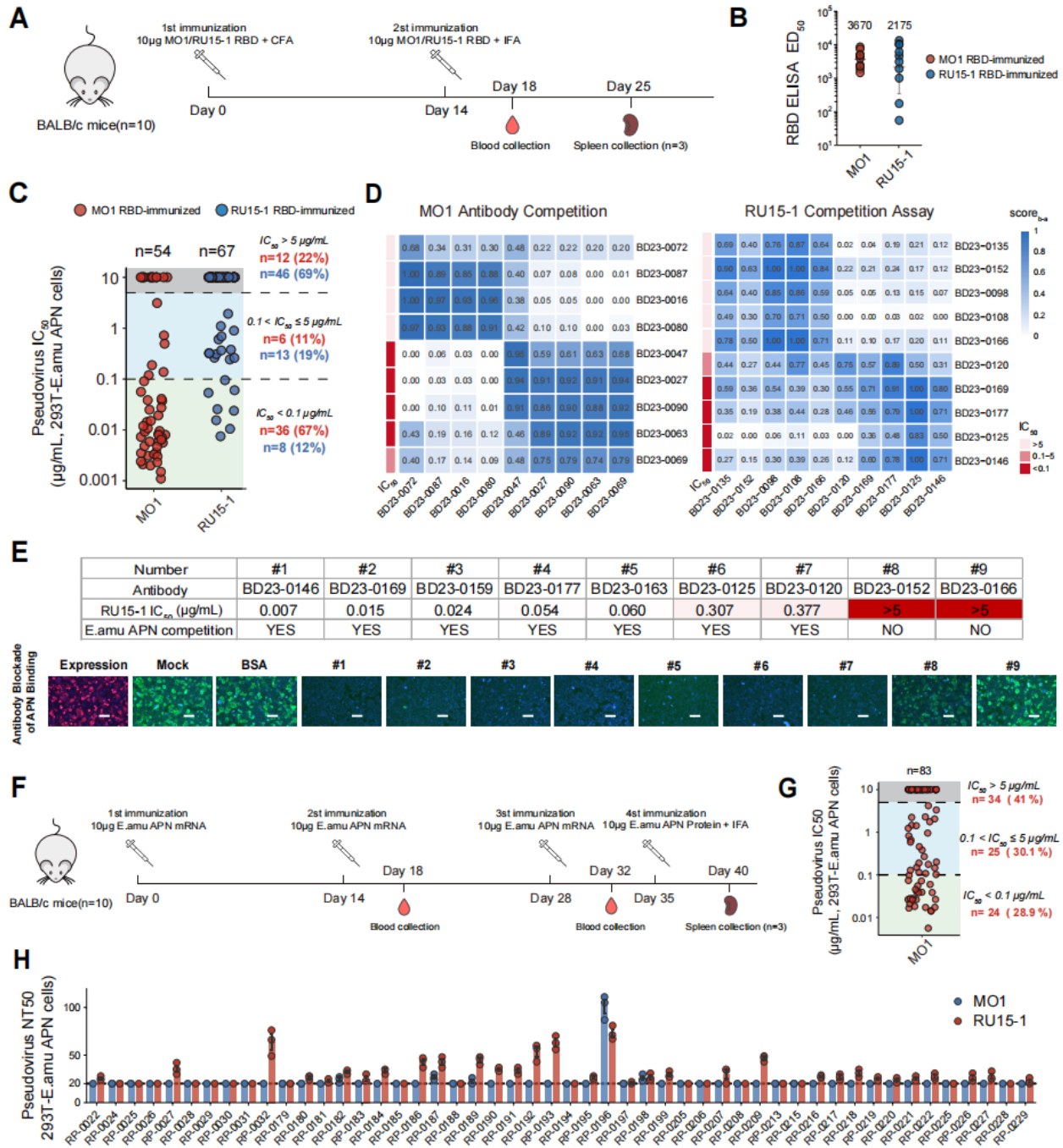
17  
18 We further validated antibody neutralization using replication-competent rcVSV-S pseudoviruses.  
19 Nine representative RU15-1 antibodies were tested against the RU15-1 and IT5-12 strains in  
20 Caco-2 cells expressing *E.amu* APN, alongside two well-characterized broadly neutralizing  
21 antibodies targeting the S2 domain as controls (Figure S6B).<sup>81,82</sup> Strongly neutralizing antibodies  
22 potently inhibited replication of both strains, while weakly neutralizing antibodies showed only  
23 marginal suppression. These results aligned closely with IC<sub>50</sub> values from single-round  
24 pseudovirus assays. Additionally, we found that all RU15-1 neutralizing mAbs could neutralize  
25 IT5-12 despite its RBD sharing only 87% sequence identity with RU15-1, suggesting conserved  
26 antigenicity among European EriCoV strains.

27  
28 Next, we analyzed the relationship between the RBD-binding epitope and EriCoV neutralization  
29 activity of the antibodies. We performed epitope binning assays using SPR competition for  
30 antibodies binding to both the MO1 and RU15-1 RBDs (Figure 6D). The antibodies from both  
31 groups segregated into two distinct epitope bins, only one of which correlated strongly with  
32 pseudovirus neutralization. To determine if neutralization was mediated by blocking the receptor  
33 binding site, we selected nine representative RU15-1 antibodies for an APN receptor competition  
34 assay (Figure 6E). Recombinant RBD-hFc proteins were pre-incubated with RBD-binding  
35 antibodies and then applied to HEK293T cells transiently expressing *E.amu* APN to evaluate  
36 antibody APN blockage efficiency. The results revealed a clear correlation between the ability of  
37 antibody-APN blockage and viral neutralization (Figure 6E), underscoring the critical role of the  
38 RBD-APN interaction for EriCoV entry.

39  
40 To further validate the role of APN as a functional receptor for EriCoV, we investigated whether  
41 antibodies targeting APN itself could block infection. Mice were immunized via intramuscular  
42 injection with 10 µg of *E.amu* APN mRNA on Days 0, 14, and 28. This was followed by a booster  
43 injection with 10 µg of purified *E.amu* APN protein formulated with incomplete Freund's adjuvant  
44 (IFA) on Day 35 (Figure 6F). Mouse spleens were collected on Day 40, and *E.amu* APN-specific  
45 single B cells were sorted. Using the method described above, we expressed APN-binding

1 antibodies from these cells. In total, we obtained 83 *E.amu* APN-binding antibodies (Table S2).  
2 Significantly, we found that over 50% of these antibodies displayed strong neutralization activity  
3 against EriCoV pseudoviruses in HEK293T-*E.amu* APN cells (Figure 6G). This result again  
4 provides direct evidence that APN is critical for EriCoV infection.

5  
6 Together, we developed potent EriCoV-neutralizing antibodies that target the viral RBD–APN  
7 interaction and demonstrated their efficacy in blocking pseudovirus entry and propagation. These  
8 neutralizing antibodies represent promising candidate therapeutics for pandemic preparedness  
9 against potential future EriCoV spillover events. This is particularly relevant given that population  
10 immunity from SARS-CoV-2 infection and vaccination history shows negligible neutralizing  
11 activity against EriCoV (Figure 6H & Table S3).



1  
2 **Figure 6 | Neutralizing antibodies efficiently block EriCoV S-mediated entry.** (A) Schematic  
3 of EriCoV RBD immunization in mice (n = 10 per group). (B) ELISA analyses of serum samples  
4 from immunized mice. ED<sub>50</sub> values were calculated using four-parameter logistic regression.  
5 Geometric mean titers (GMT), fold changes, and statistical significance were determined by two-  
6 tailed *t* test and are shown above each group. (C) Pseudovirus IC<sub>50</sub> values of monoclonal  
7 antibodies (mAbs) derived from MO1 (red circles, n = 54) or RU15-1 (blue circles, n = 67)  
8 immunization groups, categorized by potency. Neutralization assays were performed in  
9 HEK293T-*E.amu* APN cells using pseudoviruses corresponding to the respective immunogens.  
10 (D) Heatmap for pair-wise SPR competition scores of anti-RBD mAbs, with darker blue indicating  
11 stronger competition. Corresponding IC<sub>50</sub> of mAbs are represented as red bars on the left

1 heatmap, with darker red indicating higher neutralization potency. (E) Antibody blockage of APN  
2 binding of 9 representative mAbs isolated from RU15-1-immunized mice against RU15-1  
3 pseudoviruses, determined using HEK293T-*E.amu* APN cells and RBD-hFc. (F) Schematic of  
4 *E.amu* APN immunization in mice (n = 10). (G) Pseudovirus IC<sub>50</sub> values of mAbs derived from  
5 *E.amu* APN-immunized mice, categorized by potency. Neutralization assays were performed in  
6 HEK293T-*E.amu* APN cells using MO1 pseudoviruses. (H) Neutralization 50% titers of plasma  
7 samples from random human donors against MO1 and RU15-1 pseudoviruses, determined using  
8 HEK293T-*E.amu* APN cells. Dashed lines indicate the assay baseline. Scale bars: 100 μm for  
9 panel E.

10 See also Figure S6.

11

## 12 DISCUSSION

13 Coronaviruses circulating in wildlife continue to pose a significant threat of future pandemics.<sup>83,84</sup>  
14 Predicting the cross-species transmission potential of specific coronavirus strains remains  
15 challenging due to limited knowledge of their host entry and transmission mechanisms. EriCoVs  
16 as relatives of MERS-CoV have been known for over a decade and are now recognized as  
17 genetically diverse and widely distributed.<sup>25,33</sup> Unlike bats, which generally inhabit areas distant  
18 from human populations, hedgehogs often interact with humans as urban wildlife or pets.<sup>85</sup> As  
19 important members of the merbecovirus subgenus associated with potential high pathogenicity,  
20 EriCoVs remain poorly characterized in terms of their spillover risks. A key obstacle to this  
21 understanding is the lack of receptor information, which hinders cross-species risk assessment,  
22 viral isolation, pathogenesis studies, and countermeasure development.

23

24 DPP4 was first identified in 2013 as a functional receptor for MERS-CoV<sup>43</sup> and later considered  
25 the canonical receptor for merbecoviruses, especially after the identification of more DPP4-using  
26 HKU4-related viruses.<sup>15,67</sup> However, many merbecoviruses appear unable to use DPP4 orthologs  
27 from either humans or their host species.<sup>26,40,56,79</sup> A decade later, the identification of ACE2-using  
28 NeoCoV and others indicates that ACE2 is also an important receptor in mediating merbecovirus  
29 entry.<sup>40,66</sup> Subsequent discoveries of two additional independently acquired interaction modes  
30 have established ACE2 as another major receptor in this subgenus.<sup>24,50,51,55–57,86</sup> With most  
31 merbecovirus receptor usage now defined, EriCoV remained the last unresolved lineage. Notably,  
32 while EriCoV shows certain homology and similar insertion/deletion patterns with ACE2-using  
33 NeoCoV, these viruses do not appear to use ACE2.<sup>40,56</sup> Some studies proposed that DPP4 may  
34 serve as an alternative receptor for EriCoVs through *in silico* protein docking simulations; however,  
35 no functional evidence supported this hypothesis.<sup>33</sup>

36

37 Our study identifies APN as its functional receptor, unexpectedly expanding APN usage to the  
38 betacoronavirus genus. APN was initially identified as a receptor for two alphacoronaviruses,<sup>44,45</sup>  
39 each engaging it through distinct binding modes.<sup>59,73,75</sup> More recently, deltacoronaviruses like  
40 PDCoV and avian CoVs were also shown to use APN via a third binding mode.<sup>52</sup> Our findings  
41 add a fourth APN-binding mode, in which EriCoV binds exclusively to the ‘closed’ conformation  
42 of APN through a uniquely oriented RBD with a distinct footprint that evolved independently. This  
43 finding underscores the remarkable plasticity of coronavirus RBDs in adapting to diverse receptor  
44 surfaces<sup>51</sup> and illustrates the limitations of predictive modeling, as even minor sequence changes  
45 can dramatically alter receptor usage of coronaviruses.<sup>67</sup>

1  
2 The convergent utilization of APN by EriCoVs is reminiscent of the multiple independent  
3 acquisitions of ACE2 usage among coronaviruses.<sup>50,51,86</sup> These observations suggest that the  
4 acquisition of a receptor by coronaviruses is not random. Intriguingly, the three merbecovirus  
5 receptors—ACE2, DPP4, and APN—are all ectopeptidases with abundant expression on  
6 epithelial surfaces of the respiratory and gastrointestinal tracts. The repeated exploitation  
7 suggests strong evolutionary advantages, such as more efficient entry, potential for broad tissue  
8 tropism, and favorable biochemical properties for virus–receptor interaction.<sup>87</sup>

9  
10 Despite structural similarity and certain sequence homology between NeoCoV and EriCoV, their  
11 distinct receptor usage implies a receptor-switch event during their evolutionary separation. The  
12 direction and drivers of this shift remain unclear, though recombination, RBM insertions/deletions,  
13 and antigenic drift are likely contributors.<sup>68,88,89</sup> Given their shared indel patterns, antigenic drift  
14 likely played a central role. In this case, adaptive mutations in multiple interacting residues are  
15 necessary to achieve entirely different receptor recognition modes,<sup>58</sup> which aligns with their  
16 significant differences in receptor-interacting residues.

17  
18 Our results show that EriCoVs are highly adapted to hedgehog APN orthologs, with limited ability  
19 to utilize APN orthologs from humans and other species, determined by critical residues and  
20 glycosylation near the interaction interface. The strong host specialization and narrow  
21 compatibility to other APN orthologs imply a high evolutionary barrier of these viruses to zoonotic  
22 transmission under current conditions. In addition to receptor binding, other host factors like  
23 TMPRSS2 compatibility, replication efficiency, and immune responses may also influence host  
24 range. Notably, EriCoV exhibits modest ability to engage feline APN, raising the possibility that  
25 domestic cats could serve as intermediate hosts. Given the close human–cat association, it will  
26 be important to monitor feline populations, especially in areas with known hedgehog–human  
27 overlap, for signs of EriCoV exposure. To date, no spillover events have been reported, and most  
28 known EriCoVs have been isolated from *E.eur* or *E.amu* hedgehogs. Whether these viruses infect  
29 other hedgehog species or have broader host ranges remains unclear.

30  
31 Thus, continued surveillance and close monitoring of suspicious sequence changes, coupled with  
32 receptor-focused functional studies, are essential for pandemic preparedness.<sup>11,83</sup> Although  
33 receptor-switch is not common for coronaviruses, merbecoviruses are notable for their RBM  
34 plasticity,<sup>58,88,89</sup> facilitating their ability to adapt human receptors for zoonotic emergence.  
35 Development of EriCoV-specific neutralizing antibodies and vaccines could provide preemptive  
36 countermeasures. Overall, our findings expand the repertoire of receptor usage within the  
37 *merbecovirus* subgenus, providing a structural and functional basis for risk assessment and  
38 countermeasure development for those viruses that could potentially pose a threat to humans or  
39 domestic animals.

#### 40 41 **Limitations of the study**

42 Several limitations of this study should be acknowledged. First, all functional assessments of viral  
43 entry were conducted using pseudoviruses in cell-based systems, and no infection experiments  
44 with authentic viruses or *in vivo* models were performed. Moreover, due to the lack of available  
45 hedgehog-derived cell lines, we were also unable to assess viral entry in a native host cell context.

1 As such, our findings may not fully recapture the complexity of viral infection dynamics in natural  
2 hosts. Second, while we tested representative viral strains, the panel does not encompass the full  
3 genetic diversity within the lineage, and untested variants may exhibit distinct APN tropism  
4 features and protease preference. Lastly, although certain feline APN orthologs supported  
5 pseudovirus entry *in vitro*, it remains unclear whether the feline species are truly susceptible to  
6 infection *in vivo*. Receptor usage alone does not guarantee host susceptibility; other factors such  
7 as protease expression, immune barriers, and viral replication capacity also play critical roles.  
8 Future studies using authentic viruses, a broader range of viral strains, and *in vivo* challenge  
9 models will be essential to fully assess the zoonotic potential and pathogenicity of these  
10 merbecoviruses.

11

## 12 **Acknowledgments:**

13 This study was supported by the National Key R&D Program of China (2024YFC2607300 and  
14 2023YFC2605500 to H.Y.), the National Natural Science Foundation of China (NSFC) projects  
15 (82322041, 32270164 to H.Y., 323B2006 to C.-B.M.), Scientific Research Innovation Capability  
16 Support Project for Young Faculty (ZYGXONJSKYCXNLZCXM-H16 to H.Y.), Natural Science  
17 Foundation of Hubei Province (2023AFA015 to H.Y.), the Fundamental Research Funds for the  
18 Central Universities (to H.Y.), and TaiKang Center for Life and Medical Sciences (to H.Y.). This  
19 work was also supported by the Strategic Priority Research Program (XDB1310000 to X.W.),  
20 National Science Foundation Grants (32325004, T2394482, and 12034006 to X.W.), Basic  
21 Research Program Based on Major Scientific Infrastructures, CAS-JZHKYPT-2021-05, CAS  
22 (YSBR-010 to X.W.), Ministry of Science and Technology of China (CPL-1233 to X.W.), and  
23 Changping Laboratory (2025D-04-01 to Y.C.). We thank Lu Lu (Fudan University) for providing  
24 EK1C4 peptides used in this study.

25

## 26 **Author contributions:**

27 H.Y., X.W., Y.C., and P.L. conceived the project. P.L., C.M., Z.M., Q.Z., J.L., and T.L. cloned S,  
28 RBD-hFc, and APN mutants and conducted RBD-hFc binding assays. C.M., P.L., J.L., Y.Y., T.L.,  
29 and X.Yang designed APN ectodomain and antibody constructs and expressed recombinant  
30 proteins. C.L., P.L., and J.S. conducted phylogenetic and conservation analysis. Z.M., P.L., and  
31 M.H. conducted pseudovirus production and cell-cell fusion assays. Z.M., P.L., and X.Yang  
32 rescued the rcVSV-EriCoV-S pseudotypes and performed rcVSV propagation and inhibition  
33 assays. Q.Z. and T.L. conducted biolayer interferometry binding experiments. J.L., P.L., and  
34 X.Yang carried out VSV pseudovirus entry and neutralization assays. Q.Z. carried out cryo-EM  
35 sample preparation, data collection, and processing. Q.Z. and X.W. built and refined the  
36 structures. J.L., Y.Y., and Q.W. performed animal experiments and flow cytometric sorting of  
37 single B cells. Y.Y., J.L., and L.Y. conducted monoclonal antibody expression, functional  
38 characterization, and neutralization assays. P.L., Z. M., C.L., Y.S., J.S., X.Yu, J.L., and Y.X.  
39 analyzed the data. H.Y., X.W., and Y.C. wrote the manuscript with input from all authors.

40

## 41 **Competing interests:**

42 The authors declare no competing interests.

43

## 1 Reference

- 2 1. Guan, Y., Zheng, B.J., He, Y.Q., Liu, X.L., Zhuang, Z.X., Cheung, C.L., Luo, S.W., Li, P.H.,  
3 Zhang, L.J., Guan, Y.J., et al. (2003). Isolation and characterization of viruses related to the  
4 SARS coronavirus from animals in southern China. *Science* 302, 276–278.
- 5 2. Drosten, C., Günther, S., Preiser, W., van der Werf, S., Brodt, H.-R., Becker, S., Rabenau,  
6 H., Panning, M., Kolesnikova, L., Fouchier, R.A.M., et al. (2003). Identification of a novel  
7 coronavirus in patients with severe acute respiratory syndrome. *N Engl J Med* 348, 1967–  
8 1976.
- 9 3. Zaki, A.M., van Boheemen, S., Bestebroer, T.M., Osterhaus, A.D.M.E., and Fouchier,  
10 R.A.M. (2012). Isolation of a novel coronavirus from a man with pneumonia in Saudi Arabia.  
11 *N Engl J Med* 367, 1814–1820.
- 12 4. Zhu, N., Zhang, D., Wang, W., Li, X., Yang, B., Song, J., Zhao, X., Huang, B., Shi, W., Lu,  
13 R., et al. (2020). A Novel Coronavirus from Patients with Pneumonia in China, 2019. *N Engl*  
14 *J Med* 382, 727–733.
- 15 5. Zhou, P., Yang, X.-L., Wang, X.-G., Hu, B., Zhang, L., Zhang, W., Si, H.-R., Zhu, Y., Li, B.,  
16 Huang, C.-L., et al. (2020). A pneumonia outbreak associated with a new coronavirus of  
17 probable bat origin. *Nature* 579, 270–273.
- 18 6. Mallapaty, S. (2024). The pathogens that could spark the next pandemic. *Nature* 632, 488.
- 19 7. Pathogens prioritization: a scientific framework for epidemic and pandemic research  
20 preparedness [https://www.who.int/publications/m/item/pathogens-prioritization-a-scientific-](https://www.who.int/publications/m/item/pathogens-prioritization-a-scientific-framework-for-epidemic-and-pandemic-research-preparedness)  
21 [framework-for-epidemic-and-pandemic-research-preparedness](https://www.who.int/publications/m/item/pathogens-prioritization-a-scientific-framework-for-epidemic-and-pandemic-research-preparedness).
- 22 8. Ngere, I., Hunsperger, E.A., Tong, S., Oyugi, J., Jaoko, W., Harcourt, J.L., Thornburg, N.J.,  
23 Oyas, H., Muturi, M., Osoro, E.M., et al. (2022). Outbreak of Middle East Respiratory  
24 Syndrome Coronavirus in Camels and Probable Spillover Infection to Humans in Kenya.  
25 *Viruses* 14. <https://doi.org/10.3390/v14081743>.
- 26 9. Haagmans, B.L., Al Dhahiry, S.H.S., Reusken, C.B.E.M., Raj, V.S., Galiano, M., Myers, R.,  
27 Godeke, G.-J., Jonges, M., Farag, E., Diab, A., et al. (2014). Middle East respiratory  
28 syndrome coronavirus in dromedary camels: an outbreak investigation. *Lancet Infect Dis*  
29 14, 140–145.
- 30 10. Mohd, H.A., Al-Tawfiq, J.A., and Memish, Z.A. (2016). Middle East Respiratory Syndrome  
31 Coronavirus (MERS-CoV) origin and animal reservoir. *Viol J* 13, 87.
- 32 11. Tolentino, J.E., Lytras, S., Ito, J., and Sato, K. (2025). Beyond MERS: Merbecovirus  
33 receptor plasticity calls for emergence preparedness. *Cell Host Microbe* 33, 453–456.
- 34 12. Cui, J., Li, F., and Shi, Z.-L. (2019). Origin and evolution of pathogenic coronaviruses. *Nat*  
35 *Rev Microbiol* 17, 181–192.
- 36 13. Ithete, N.L., Stoffberg, S., Corman, V.M., Cottontail, V.M., Richards, L.R., Schoeman, M.C.,  
37 Drosten, C., Drexler, J.F., and Preiser, W. (2013). Close relative of human Middle East  
38 respiratory syndrome coronavirus in bat, South Africa. *Emerg Infect Dis* 19, 1697–1699.
- 39 14. Wang, Q., Qi, J., Yuan, Y., Xuan, Y., Han, P., Wan, Y., Ji, W., Li, Y., Wu, Y., Wang, J., et  
40 al. (2014). Bat origins of MERS-CoV supported by bat coronavirus HKU4 usage of human

- 1 receptor CD26. *Cell Host Microbe* *16*, 328–337.
- 2 15. Yang, Y., Du, L., Liu, C., Wang, L., Ma, C., Tang, J., Baric, R.S., Jiang, S., and Li, F.  
3 (2014). Receptor usage and cell entry of bat coronavirus HKU4 provide insight into bat-to-  
4 human transmission of MERS coronavirus. *Proc Natl Acad Sci U S A* *111*, 12516–12521.
- 5 16. Corman, V.M., Ithete, N.L., Richards, L.R., Schoeman, M.C., Preiser, W., Drosten, C., and  
6 Drexler, J.F. (2014). Rooting the phylogenetic tree of middle East respiratory syndrome  
7 coronavirus by characterization of a conspecific virus from an African bat. *J Virol* *88*,  
8 11297–11303.
- 9 17. Luo, C.-M., Wang, N., Yang, X.-L., Liu, H.-Z., Zhang, W., Li, B., Hu, B., Peng, C., Geng, Q.-  
10 B., Zhu, G.-J., et al. (2018). Discovery of Novel Bat Coronaviruses in South China That Use  
11 the Same Receptor as Middle East Respiratory Syndrome Coronavirus. *J Virol* *92*.  
12 <https://doi.org/10.1128/JVI.00116-18>.
- 13 18. Lau, S.K.P., Zhang, L., Luk, H.K.H., Xiong, L., Peng, X., Li, K.S.M., He, X., Zhao, P.S.-H.,  
14 Fan, R.Y.Y., Wong, A.C.P., et al. (2018). Receptor Usage of a Novel Bat Lineage C  
15 Betacoronavirus Reveals Evolution of Middle East Respiratory Syndrome-Related  
16 Coronavirus Spike Proteins for Human Dipeptidyl Peptidase 4 Binding. *J Infect Dis* *218*,  
17 197–207.
- 18 19. Alagaili, A.N., Briese, T., Mishra, N., Kapoor, V., Sameroff, S.C., Burbelo, P.D., de Wit, E.,  
19 Munster, V.J., Hensley, L.E., Zalmout, I.S., et al. (2014). Middle East respiratory syndrome  
20 coronavirus infection in dromedary camels in Saudi Arabia. *mBio* *5*, e00884–14.
- 21 20. Meyer, B., Müller, M.A., Corman, V.M., Reusken, C.B.E.M., Ritz, D., Godeke, G.-J.,  
22 Lattwein, E., Kallies, S., Siemens, A., van Beek, J., et al. (2014). Antibodies against MERS  
23 coronavirus in dromedary camels, United Arab Emirates, 2003 and 2013. *Emerg Infect Dis*  
24 *20*, 552–559.
- 25 21. Azhar, E.I., El-Kafrawy, S.A., Farraj, S.A., Hassan, A.M., Al-Saeed, M.S., Hashem, A.M.,  
26 and Madani, T.A. (2014). Evidence for camel-to-human transmission of MERS coronavirus.  
27 *N Engl J Med* *370*, 2499–2505.
- 28 22. Xia, L.-Y., Wang, Z.-F., Cui, X.-M., Li, Y.-G., Ye, R.-Z., Zhu, D.-Y., Li, F.-X., Zhang, J.,  
29 Wang, W.-H., Zhang, M.-Z., et al. (2024). Isolation and characterization of a pangolin-borne  
30 HKU4-related coronavirus that potentially infects human-DPP4-transgenic mice. *Nat*  
31 *Commun* *15*, 1048.
- 32 23. Chen, J., Yang, X., Si, H., Gong, Q., Que, T., Li, J., Li, Y., Wu, C., Zhang, W., Chen, Y., et  
33 al. (2023). A bat MERS-like coronavirus circulates in pangolins and utilizes human DPP4  
34 and host proteases for cell entry. *Cell* *186*, 850–863.e16.
- 35 24. Wang, N., Ji, W., Jiao, H., Veit, M., Sun, J., Wang, Y., Ma, X., Wang, Y., Wang, Y., Li, X.-  
36 X., et al. (2025). A MERS-CoV-like mink coronavirus uses ACE2 as an entry receptor.  
37 *Nature* *642*, 739–746.
- 38 25. Corman, V.M., Kallies, R., Philipps, H., Göpner, G., Müller, M.A., Eckerle, I., Brünink, S.,  
39 Drosten, C., and Drexler, J.F. (2014). Characterization of a novel betacoronavirus related to  
40 middle East respiratory syndrome coronavirus in European hedgehogs. *J Virol* *88*, 717–  
41 724.

- 1 26. Lau, S.K.P., Luk, H.K.H., Wong, A.C.P., Fan, R.Y.Y., Lam, C.S.F., Li, K.S.M., Ahmed, S.S.,  
2 Chow, F.W.N., Cai, J.-P., Zhu, X., et al. (2019). Identification of a Novel Betacoronavirus ()  
3 in Amur Hedgehogs from China. *Viruses* *11*. <https://doi.org/10.3390/v11110980>.
- 4 27. Beissat, K., Picard-Meyer, E., Arné, P., Chanteclair, F., Le Barzic, C., Hivert, L., Le Loc'h,  
5 G., Puech, M.-P., Bastien, F., Schereffer, J.-L., et al. (2025). Coding-complete genome  
6 sequences of hedgehog coronavirus isolated from in France. *Microbiol Resour Announc* *14*,  
7 e0015725.
- 8 28. Saldanha, I.F., Lawson, B., Goharriz, H., Rodriguez-Ramos Fernandez, J., John, S.K.,  
9 Fooks, A.R., Cunningham, A.A., Johnson, N., and Horton, D.L. (2019). Extension of the  
10 known distribution of a novel clade C betacoronavirus in a wildlife host. *Epidemiol Infect*  
11 *147*, e169.
- 12 29. De Sabato, L., Di Bartolo, I., De Marco, M.A., Moreno, A., Lelli, D., Cotti, C., Delogu, M.,  
13 and Vaccari, G. (2020). Can Coronaviruses Steal Genes from the Host as Evidenced in  
14 Western European Hedgehogs by EriCoV Genetic Characterization? *Viruses* *12*.  
15 <https://doi.org/10.3390/v12121471>.
- 16 30. Delogu, M., Cotti, C., Lelli, D., Sozzi, E., Trogu, T., Lavazza, A., Garuti, G., Castrucci, M.R.,  
17 Vaccari, G., De Marco, M.A., et al. (2020). Eco-Virological Preliminary Study of Potentially  
18 Emerging Pathogens in Hedgehogs () Recovered at a Wildlife Treatment and Rehabilitation  
19 Center in Northern Italy. *Animals (Basel)* *10*. <https://doi.org/10.3390/ani10030407>.
- 20 31. Domanska-Blicharz, K., Lisowska, A., Opolska, J., Ruzskowski, J.J., Gogulski, M., and  
21 Pomorska-Mól, M. (2024). Whole genome characteristics of hedgehog coronaviruses from  
22 Poland and analysis of the evolution of the Spike protein for its interspecies transmission  
23 potential. *BMC Vet Res* *20*, 424.
- 24 32. Pomorska-Mól, M., Ruzskowski, J.J., Gogulski, M., and Domanska-Blicharz, K. (2022). First  
25 detection of Hedgehog coronavirus 1 in Poland. *Sci Rep* *12*, 2386.
- 26 33. Cruz, A.V.S., Santos-Silva, S., Queirós-Reis, L., Rodrigues, C., Soeiro, V., Tarlinton, R.E.,  
27 and Mesquita, J.R. (2024). Genomic characterization and cross-species transmission  
28 potential of hedgehog coronavirus. *One Health* *19*, 100940.
- 29 34. Lukina-Gronskaya, A.V., Chudinov, I.K., Korneenko, E.V., Mashkova, S.D., Semashko,  
30 T.A., Sinkova, M.A., Penkin, L.N., Litvinova, E.M., Feoktistova, N.Y., and Speranskaya,  
31 A.S. (2024). Novel coronaviruses and mammarenaviruses of hedgehogs from Russia  
32 including the comparison of viral communities of hibernating and active specimens. *Front*  
33 *Vet Sci* *11*, 1486635.
- 34 35. He, W.-T., Hou, X., Zhao, J., Sun, J., He, H., Si, W., Wang, J., Jiang, Z., Yan, Z., Xing, G.,  
35 et al. (2022). Virome characterization of game animals in China reveals a spectrum of  
36 emerging pathogens. *Cell* *185*, 1117–1129.e8.
- 37 36. Li, D., Gong, X.-Q., Xiao, X., Han, H.-J., Yu, H., Li, Z.-M., Yan, L.-N., Gu, X.-L., Duan, S.-  
38 H., and Xue-jieYu (2021). MERS-related CoVs in hedgehogs from Hubei Province, China.  
39 *One Health* *13*, 100332.
- 40 37. Lu, G., Wang, Q., and Gao, G.F. (2015). Bat-to-human: spike features determining “host  
41 jump” of coronaviruses SARS-CoV, MERS-CoV, and beyond. *Trends Microbiol.* *23*, 468–  
42 478.

- 1 38. Dveksler, G.S., Pensiero, M.N., Cardellichio, C.B., Williams, R.K., Jiang, G.S., Holmes,  
2 K.V., and Dieffenbach, C.W. (1991). Cloning of the mouse hepatitis virus (MHV) receptor:  
3 expression in human and hamster cell lines confers susceptibility to MHV. *J Virol* 65, 6881–  
4 6891.
- 5 39. Williams, R.K., Jiang, G.S., and Holmes, K.V. (1991). Receptor for mouse hepatitis virus is  
6 a member of the carcinoembryonic antigen family of glycoproteins. *Proc Natl Acad Sci U S*  
7 *A* 88, 5533–5536.
- 8 40. Xiong, Q., Cao, L., Ma, C., Tortorici, M.A., Liu, C., Si, J., Liu, P., Gu, M., Walls, A.C., Wang,  
9 C., et al. (2022). Close relatives of MERS-CoV in bats use ACE2 as their functional  
10 receptors. *Nature* 612, 748–757.
- 11 41. Hofmann, H., Pyrc, K., van der Hoek, L., Geier, M., Berkhout, B., and Pöhlmann, S. (2005).  
12 Human coronavirus NL63 employs the severe acute respiratory syndrome coronavirus  
13 receptor for cellular entry. *Proc Natl Acad Sci U S A* 102, 7988–7993.
- 14 42. Li, W., Moore, M.J., Vasilieva, N., Sui, J., Wong, S.K., Berne, M.A., Somasundaran, M.,  
15 Sullivan, J.L., Luzuriaga, K., Greenough, T.C., et al. (2003). Angiotensin-converting enzyme  
16 2 is a functional receptor for the SARS coronavirus. *Nature* 426, 450–454.
- 17 43. Raj, V.S., Mou, H., Smits, S.L., Dekkers, D.H.W., Müller, M.A., Dijkman, R., Muth, D.,  
18 Demmers, J.A.A., Zaki, A., Fouchier, R.A.M., et al. (2013). Dipeptidyl peptidase 4 is a  
19 functional receptor for the emerging human coronavirus-EMC. *Nature* 495, 251–254.
- 20 44. Yeager, C.L., Ashmun, R.A., Williams, R.K., Cardellichio, C.B., Shapiro, L.H., Look, A.T.,  
21 and Holmes, K.V. (1992). Human aminopeptidase N is a receptor for human coronavirus  
22 229E. *Nature* 357, 420–422.
- 23 45. Delmas, B., Gelfi, J., L'Haridon, R., Vogel, L.K., Sjöström, H., Norén, O., and Laude, H.  
24 (1992). Aminopeptidase N is a major receptor for the entero-pathogenic coronavirus TGEV.  
25 *Nature* 357, 417–420.
- 26 46. Wang, H., Liu, X., Zhang, X., Zhao, Z., Lu, Y., Pu, D., Zhang, Z., Chen, J., Wang, Y., Li, M.,  
27 et al. (2024). TMPRSS2 and glycan receptors synergistically facilitate coronavirus entry.  
28 *Cell* 187, 4261–4271.e17.
- 29 47. McCallum, M., Park, Y.-J., Stewart, C., Sprouse, K.R., Addetia, A., Brown, J., Tortorici,  
30 M.A., Gibson, C., Wong, E., Ieven, M., et al. (2024). Human coronavirus HKU1 recognition  
31 of the TMPRSS2 host receptor. *Cell* 187, 4231–4245.e13.
- 32 48. Fernández, I., Saunders, N., Duquerroy, S., Bolland, W.H., Arbabian, A., Baquero, E.,  
33 Blanc, C., Lafaye, P., Haouz, A., Buchrieser, J., et al. (2024). Structural basis of TMPRSS2  
34 zymogen activation and recognition by the HKU1 seasonal coronavirus. *Cell* 187, 4246–  
35 4260.e16.
- 36 49. Saunders, N., Fernandez, I., Planchais, C., Michel, V., Rajah, M.M., Baquero Salazar, E.,  
37 Postal, J., Porrot, F., Guivel-Benhassine, F., Blanc, C., et al. (2023). TMPRSS2 is a  
38 functional receptor for human coronavirus HKU1. *Nature* 624, 207–214.
- 39 50. Park, Y.-J., Liu, C., Lee, J., Brown, J.T., Ma, C.-B., Liu, P., Gen, R., Xiong, Q., Zepeda,  
40 S.K., Stewart, C., et al. (2025). Molecular basis of convergent evolution of ACE2 receptor  
41 utilization among HKU5 coronaviruses. *Cell* 188, 1711–1728.e21.

- 1 51. Ma, C.-B., Liu, C., Park, Y.-J., Tang, J., Chen, J., Xiong, Q., Lee, J., Stewart, C., Asarnow,  
2 D., Brown, J., et al. (2025). Multiple independent acquisitions of ACE2 usage in MERS-  
3 related coronaviruses. *Cell* *188*, 1693–1710.e18.
- 4 52. Ji, W., Peng, Q., Fang, X., Li, Z., Li, Y., Xu, C., Zhao, S., Li, J., Chen, R., Mo, G., et al.  
5 (2022). Structures of a deltacoronavirus spike protein bound to porcine and human  
6 receptors. *Nat Commun* *13*, 1467.
- 7 53. Walls, A.C., Park, Y.-J., Tortorici, M.A., Wall, A., McGuire, A.T., and Velesler, D. (2020).  
8 Structure, Function, and Antigenicity of the SARS-CoV-2 Spike Glycoprotein. *Cell* *181*,  
9 281–292.e6.
- 10 54. Hoffmann, M., Kleine-Weber, H., Schroeder, S., Krüger, N., Herrler, T., Erichsen, S.,  
11 Schiergens, T.S., Herrler, G., Wu, N.-H., Nitsche, A., et al. (2020). SARS-CoV-2 Cell Entry  
12 Depends on ACE2 and TMPRSS2 and Is Blocked by a Clinically Proven Protease Inhibitor.  
13 *Cell* *181*, 271–280.e8.
- 14 55. Madel Alfajaro, M., Keeler, E.L., Li, N., Catanzaro, N.J., Teng, I.-T., Zhao, Z., Grunst, M.W.,  
15 Yount, B., Schäfer, A., Wang, D., et al. (2025). HKU5 bat merbecoviruses engage bat and  
16 mink ACE2 as entry receptors. *Nat Commun* *16*, 6822.
- 17 56. Catanzaro, N.J., Wu, Z., Fan, C., Jefferson, V., Abdelgadir, A., Schäfer, A., Yount, B.L.,  
18 Bjorkman, P.J., Baric, R., and Letko, M. (2025). ACE2 from *Pipistrellus abramus* bats is a  
19 receptor for HKU5 coronaviruses. *Nat Commun* *16*, 4932.
- 20 57. Chen, J., Zhang, W., Li, Y., Liu, C., Dong, T., Chen, H., Wu, C., Su, J., Li, B., Zhang, W., et  
21 al. (2025). Bat-infecting merbecovirus HKU5-CoV lineage 2 can use human ACE2 as a cell  
22 entry receptor. *Cell* *188*, 1729–1742.e16.
- 23 58. Liu, C., Park, Y.-J., Ma, C.-B., Stuart, C., Gen, R., Sun, Y.-C., Yang, X., Lin, M.-Y., Xiong,  
24 Q., Si, J.-Y., et al. (2025). ACE2 utilization of HKU25 clade MERS-related coronaviruses  
25 with broad geographic distribution. *bioRxiv*. <https://doi.org/10.1101/2025.02.19.639017>.
- 26 59. Tortorici, M.A., Walls, A.C., Joshi, A., Park, Y.-J., Eguia, R.T., Miranda, M.C., Kepl, E.,  
27 Dosey, A., Stevens-Ayers, T., Boeckh, M.J., et al. (2022). Structure, receptor recognition,  
28 and antigenicity of the human coronavirus CCoV-HuPn-2018 spike glycoprotein. *Cell* *185*,  
29 2279–2291.e17.
- 30 60. Tortorici, M.A., Choi, A., Gibson, C.A., Lee, J., Brown, J.T., Stewart, C., Joshi, A., Harari,  
31 S., Willoughby, I., Treichel, C., et al. (2025). Loss of FCoV-23 spike domain 0 enhances  
32 fusogenicity and entry kinetics. *Nature*. <https://doi.org/10.1038/s41586-025-09155-z>.
- 33 61. Li, W., Hulswit, R.J.G., Kenney, S.P., Widjaja, I., Jung, K., Alhamo, M.A., van Dieren, B.,  
34 van Kuppeveld, F.J.M., Saif, L.J., and Bosch, B.-J. (2018). Broad receptor engagement of  
35 an emerging global coronavirus may potentiate its diverse cross-species transmissibility.  
36 *Proc Natl Acad Sci U S A* *115*, E5135–E5143.
- 37 62. Liang, Q.-Z., Wang, B., Ji, C.-M., Hu, F., Qin, P., Feng, Y., Tang, Y.-D., and Huang, Y.-W.  
38 (2023). Chicken or Porcine Aminopeptidase N Mediates Cellular Entry of Pseudoviruses  
39 Carrying Spike Glycoprotein from the Avian Deltacoronaviruses HKU11, HKU13, and  
40 HKU17. *J Virol* *97*, e0194722.
- 41 63. Shirato, K., Kawase, M., and Matsuyama, S. (2013). Middle East respiratory syndrome

- 1 coronavirus infection mediated by the transmembrane serine protease TMPRSS2. *J Virol*  
2 87, 12552–12561.
- 3 64. Bertram, S., Dijkman, R., Habjan, M., Heurich, A., Gierer, S., Glowacka, I., Welsch, K.,  
4 Winkler, M., Schneider, H., Hofmann-Winkler, H., et al. (2013). TMPRSS2 activates the  
5 human coronavirus 229E for cathepsin-independent host cell entry and is expressed in viral  
6 target cells in the respiratory epithelium. *J Virol* 87, 6150–6160.
- 7 65. Glowacka, I., Bertram, S., Müller, M.A., Allen, P., Soilleux, E., Pfefferle, S., Steffen, I.,  
8 Tsegaye, T.S., He, Y., Gnirss, K., et al. (2011). Evidence that TMPRSS2 activates the  
9 severe acute respiratory syndrome coronavirus spike protein for membrane fusion and  
10 reduces viral control by the humoral immune response. *J Virol* 85, 4122–4134.
- 11 66. Ma, C., Liu, C., Xiong, Q., Gu, M., Shi, L., Wang, C., Si, J., Tong, F., Liu, P., Huang, M., et  
12 al. (2023). Broad host tropism of ACE2-using MERS-related coronaviruses and  
13 determinants restricting viral recognition. *Cell Discov* 9, 57.
- 14 67. Yuan, H., Wang, J., Ma, Y., Li, Z., Gao, X., Habib, G., Liu, B., Chen, J., He, J., Zhou, P., et  
15 al. (2025). Structures and receptor binding activities of merbecovirus spike proteins reveal  
16 key signatures for human DPP4 adaptation. *Sci Adv* 11, eadv7296.
- 17 68. Si, J.-Y., Chen, Y.-M., Sun, Y.-H., Gu, M.-X., Huang, M.-L., Shi, L.-L., Yu, X., Yang, X.,  
18 Xiong, Q., Ma, C.-B., et al. (2024). Sarbecovirus RBD indels and specific residues dictating  
19 multi-species ACE2 adaptiveness. *Nat Commun* 15, 8869.
- 20 69. Wang, Y., Song, F., Zhu, J., Zhang, S., Yang, Y., Chen, T., Tang, B., Dong, L., Ding, N.,  
21 Zhang, Q., et al. (2017). GSA: Genome Sequence Archive. *Genomics Proteomics*  
22 *Bioinformatics* 15, 14–18.
- 23 70. Kolb, A.F., Maile, J., Heister, A., and Siddell, S.G. (1996). Characterization of functional  
24 domains in the human coronavirus HCV 229E receptor. *J Gen Virol* 77 ( Pt 10), 2515–2521.
- 25 71. Chen, L., Lin, Y.-L., Peng, G., and Li, F. (2012). Structural basis for multifunctional roles of  
26 mammalian aminopeptidase N. *Proceedings of the National Academy of Sciences* 109,  
27 17966–17971.
- 28 72. Tsai, Y.-X., Chien, Y.-C., Hsu, M.-F., Khoo, K.-H., and Hsu, S.-T.D. (2025). Molecular basis  
29 of host recognition of human coronavirus 229E. *Nature Communications* 16, 1–15.
- 30 73. Wong, A.H.M., Tomlinson, A.C.A., Zhou, D., Satkunarajah, M., Chen, K., Sharon, C.,  
31 Desforjes, M., Talbot, P.J., and Rini, J.M. (2017). Receptor-binding loops in  
32 alphacoronavirus adaptation and evolution. *Nat Commun* 8, 1735.
- 33 74. Tian, Y., Sun, J., Hou, X., Liu, Z., Chen, Z., Pan, X., Wang, Y., Ren, J., Zhang, D., Yang,  
34 B., et al. (2025). Cross-species recognition of two porcine coronaviruses to their cellular  
35 receptor aminopeptidase N of dogs and seven other species. *PLoS Pathog* 21, e1012836.
- 36 75. Reguera, J., Santiago, C., Mudgal, G., Ordoño, D., Enjuanes, L., and Casasnovas, J.M.  
37 (2012). Structural bases of coronavirus attachment to host aminopeptidase N and its  
38 inhibition by neutralizing antibodies. *PLoS Pathog* 8, e1002859.
- 39 76. Li, F., Li, W., Farzan, M., and Harrison, S.C. (2005). Structure of SARS coronavirus spike  
40 receptor-binding domain complexed with receptor. *Science* 309, 1864–1868.

- 1 77. Guo, H., Li, A., Dong, T.-Y., Su, J., Yao, Y.-L., Zhu, Y., Shi, Z.-L., and Letko, M. (2022).  
2 ACE2-Independent Bat Sarbecovirus Entry and Replication in Human and Bat Cells. *mBio*  
3 13, e0256622.
- 4 78. Letko, M., Marzi, A., and Munster, V. (2020). Functional assessment of cell entry and  
5 receptor usage for SARS-CoV-2 and other lineage B betacoronaviruses. *Nat Microbiol* 5,  
6 562–569.
- 7 79. Menachery, V.D., Dinnon, K.H., 3rd, Yount, B.L., Jr, McAnarney, E.T., Gralinski, L.E., Hale,  
8 A., Graham, R.L., Scobey, T., Anthony, S.J., Wang, L., et al. (2020). Trypsin Treatment  
9 Unlocks Barrier for Zoonotic Bat Coronavirus Infection. *J Virol* 94.  
10 <https://doi.org/10.1128/JVI.01774-19>.
- 11 80. Riva, L., Yuan, S., Yin, X., Martin-Sancho, L., Matsunaga, N., Pache, L., Burgstaller-  
12 Muehlbacher, S., De Jesus, P.D., Teriete, P., Hull, M.V., et al. (2020). Discovery of SARS-  
13 CoV-2 antiviral drugs through large-scale compound repurposing. *Nature* 586, 113–119.
- 14 81. Pinto, D., Sauer, M.M., Czudnochowski, N., Low, J.S., Tortorici, M.A., Housley, M.P.,  
15 Noack, J., Walls, A.C., Bowen, J.E., Guarino, B., et al. (2021). Broad betacoronavirus  
16 neutralization by a stem helix-specific human antibody. *Science* 373, 1109–1116.
- 17 82. Sun, X., Yi, C., Zhu, Y., Ding, L., Xia, S., Chen, X., Liu, M., Gu, C., Lu, X., Fu, Y., et al.  
18 (2022). Neutralization mechanism of a human antibody with pan-coronavirus reactivity  
19 including SARS-CoV-2. *Nat Microbiol* 7, 1063–1074.
- 20 83. Jiang, S., and Wu, F. (2025). Global surveillance and countermeasures for ACE2-using  
21 MERS-related coronaviruses with spillover risk. *Cell* 188, 1465–1468.
- 22 84. Shivaprakash, K.N., Sen, S., Paul, S., Kiesecker, J.M., and Bawa, K.S. (2021). Mammals,  
23 wildlife trade, and the next global pandemic. *Curr Biol* 31, 3671–3677.e3.
- 24 85. Ruzskowski, J.J., Hetman, M., Turlewicz-Podbielska, H., and Pomorska-Mól, M. (2021).  
25 Hedgehogs as a Potential Source of Zoonotic Pathogens-A Review and an Update of  
26 Knowledge. *Animals (Basel)* 11. <https://doi.org/10.3390/ani11061754>.
- 27 86. Xiong, Q., Ma, C., Liu, C., Tong, F., Huang, M., and Yan, H. (2024). ACE2-using  
28 merbecoviruses: Further evidence of convergent evolution of ACE2 recognition by NeoCoV  
29 and other MERS-CoV related viruses. *Cell Insight* 3, 100145.
- 30 87. Liu, P., Huang, M.-L., Guo, H., McCallum, M., Si, J.-Y., Chen, Y.-M., Wang, C.-L., Yu, X.,  
31 Shi, L.-L., Xiong, Q., et al. (2024). Design of customized coronavirus receptors. *Nature* 635,  
32 978–986.
- 33 88. Tolentino, J.E., Lytras, S., Ito, J., Holmes, E.C., and Sato, K. (2024). Recombination as an  
34 evolutionary driver of MERS-related coronavirus emergence. *Lancet Infect Dis* 24, e546.
- 35 89. Tolentino, J.E., Lytras, S., Ito, J., and Sato, K. (2024). Recombination analysis on the  
36 receptor switching event of MERS-CoV and its close relatives: implications for the  
37 emergence of MERS-CoV. *Virol J* 21, 84.
- 38 90. Götzke, H., Kilisch, M., Martínez-Carranza, M., Sograte-Idrissi, S., Rajavel, A.,  
39 Schlichthaerle, T., Engels, N., Jungmann, R., Stenmark, P., Opazo, F., et al. (2019). The  
40 ALFA-tag is a highly versatile tool for nanobody-based bioscience applications. *Nat*  
41 *Commun* 10, 4403.

- 1 91. Krissinel, E., and Henrick, K. (2007). Inference of macromolecular assemblies from  
2 crystalline state. *J. Mol. Biol.* **372**, 774–797.
- 3 92. Thompson, J.D., Gibson, T.J., and Higgins, D.G. (2002). Multiple sequence alignment using  
4 ClustalW and ClustalX. *Curr. Protoc. Bioinformatics* *Chapter 2*, Unit 2.3.
- 5 93. Nakamura, T., Yamada, K.D., Tomii, K., and Katoh, K. (2018). Parallelization of MAFFT for  
6 large-scale multiple sequence alignments. *Bioinformatics* **34**, 2490–2492.
- 7 94. Kearse, M., Moir, R., Wilson, A., Stones-Havas, S., Cheung, M., Sturrock, S., Buxton, S.,  
8 Cooper, A., Markowitz, S., Duran, C., et al. (2012). Geneious Basic: an integrated and  
9 extendable desktop software platform for the organization and analysis of sequence data.  
10 *Bioinformatics* **28**, 1647–1649.
- 11 95. Schwegmann-Weßels, C., Glende, J., Ren, X., Qu, X., Deng, H., Enjuanes, L., and Herrler,  
12 G. (2009). Comparison of vesicular stomatitis virus pseudotyped with the S proteins from a  
13 porcine and a human coronavirus. *J Gen Virol* **90**, 1724–1729.
- 14 96. Zhu, Q., Liu, P., Liu, S., Yue, C., and Wang, X. (2024). Enhancing RBD exposure and S1  
15 shedding by an extremely conserved SARS-CoV-2 NTD epitope. *Signal Transduction and*  
16 *Targeted Therapy* **9**, 1–3.
- 17 97. Yue, C., Liu, S., Meng, B., Fan, K., Yang, S., Liu, P., Zhu, Q., Mao, X., Yu, Y., Shao, F., et  
18 al. (2024). Deletion of V483 in the spike confers evolutionary advantage on SARS-CoV-2  
19 for human adaptation and host-range expansion after a prolonged pandemic. *Cell*  
20 *Research* **34**, 739–742.
- 21 98. Wang, K., Jia, Z., Bao, L., Wang, L., Cao, L., Chi, H., Hu, Y., Li, Q., Zhou, Y., Jiang, Y., et  
22 al. (2022). Memory B cell repertoire from triple vaccinees against diverse SARS-CoV-2  
23 variants. *Nature* **603**, 919–925.
- 24 99. Cao, Y., Song, W., Wang, L., Liu, P., Yue, C., Jian, F., Yu, Y., Yisimayi, A., Wang, P.,  
25 Wang, Y., et al. (2022). Characterization of the enhanced infectivity and antibody evasion of  
26 Omicron BA.2.75. *Cell Host Microbe* **30**, 1527–1539.e5.
- 27 100. Liu, P., Yue, C., Meng, B., Xiao, T., Yang, S., Liu, S., Jian, F., Zhu, Q., Yu, Y., Ren, Y., et  
28 al. (2024). Spike N354 glycosylation augments SARS-CoV-2 fitness for human adaptation  
29 through structural plasticity. *Natl Sci Rev* **11**, nwae206.
- 30 101. Gctf: Real-time CTF determination and correction (2016). *Journal of Structural Biology* **193**,  
31 1–12.
- 32 102. Punjani, A., Rubinstein, J.L., Fleet, D.J., and Brubaker, M.A. (2017). cryoSPARC:  
33 algorithms for rapid unsupervised cryo-EM structure determination. *Nature Methods* **14**,  
34 290–296.
- 35 103. Kucukelbir, A., Sigworth, F.J., and Tagare, H.D. (2013). Quantifying the local resolution of  
36 cryo-EM density maps. *Nature Methods* **11**, 63–65.
- 37 104. Pettersen, E.F., Goddard, T.D., Huang, C.C., Couch, G.S., Greenblatt, D.M., Meng, E.C.,  
38 and Ferrin, T.E. (2004). UCSF Chimera—A visualization system for exploratory research  
39 and analysis. *Journal of Computational Chemistry* **25**, 1605–1612.
- 40 105. Emsley, P., and Cowtan, K. (2004). Coot: model-building tools for molecular graphics. *Acta*

- 1 Crystallogr D Biol Crystallogr 60, 2126–2132.
- 2 106. Adams, P.D., Afonine, P.V., Bunkóczi, G., Chen, V.B., Davis, I.W., Echols, N., Headd, J.J.,  
3 Hung, L.-W., Kapral, G.J., Grosse-Kunstleve, R.W., et al. (2010). PHENIX: a  
4 comprehensive Python-based system for macromolecular structure solution. Acta  
5 Crystallogr D Biol Crystallogr 66, 213–221.
- 6 107. Nguyen, L.-T., Schmidt, H.A., von Haeseler, A., and Minh, B.Q. (2015). IQ-TREE: a fast  
7 and effective stochastic algorithm for estimating maximum-likelihood phylogenies. Mol. Biol.  
8 Evol. 32, 268–274.

9  
10

11 **STAR ★ METHODS**

12 **KEY RESOURCES TABLE**

REAGENT or RESOURCE	SOURCE	IDENTIFIER
<b>Antibodies</b>		
Alexa Fluor 488-conjugated goat anti-human IgG	Thermo Fisher Scientific	Cat#A11013
Mouse anti-FLAG antibody M2	Sigma-Aldrich	Cat#F1804
Anti-VSV-M(23H12)Antibody	kerafast	Cat# EB0011
Anti-HA-tag mAb	MBL	Cat#MBL-M180-3
Goat anti-Mouse IgG (H+L) Highly Cross-Adsorbed, Alexa Fluor Plus 594+	Thermo Fisher Scientific	Cat#A32742
β-Tubulin mAb	YEASEN	Cat#T6305200
His tag, mouse mAb	YEASEN	Cat#30101ES50
Anti-ALFA tag nanobody		N/A
76E1	Sun et al. <sup>82</sup>	N/A
S2P6	Pinto et al. <sup>81</sup>	N/A
<b>Bacterial and virus strains</b>		
VVT7	Mingzhou Chen's lab, Hubei University	N/A
VSV-dG-fLuc-GFP	Ma et al. <sup>66</sup>	N/A
<b>Chemicals, peptides, and recombinant proteins</b>		
TPCK-treated trypsin	Sigma-Aldrich	Cat#T8802
Trypsin	Sigma-Aldrich	Cat#T4549
Polybrene	Beyotime	Cat#C0351
Dulbecco's Modified Eagle Medium	Monad, China	Cat#CC00101S

Penicillin/Streptomycin	Biosharp	Cat#BL505A
Fetal Bovine Serum	Excell	Cat#FSP500-111323
GeneTwin reagent	Biomed	Cat#TG101
Lipo 2000	Biosharp	Cat#BL623E
Trypsin-EDTA (0.25%)	Gibco	Cat#25200072
SMM 293-TII Expression Medium	Sino Biological	Cat#M293TII
Pierce Protein A/G Plus Agarose	Thermo Scientific	Cat#20424
1M Tris-HCl, pH 8.0	Thermo Scientific	Cat#15568025
Strep-Tactin XT 4Flow high-capacity resin	IBA	Cat#2-5030-002
Hanks' Balanced Salt Solution	ServiceBio	Cat#G4204
Poly-L-lysine hydrobromide	Sigma	Cat#P1399
PMSF	Beyotime	Cat#ST506
Triton X-100	Solarbio	Cat#T8200
GelGreen	Biosharp	Cat#BS355A
D-Biotin	Shanghai yuanye Bio-Technology Co., Ltd	Cat#S13004
EK1C4 peptide	LuLu's lab, Fudan University	N/A
E64d	Aladdin	Cat#E123225
Camostat	MedChemExpress	Cat#HY-13512
Critical commercial assays		
Bright-Glo Luciferase Assay Kit	Promega	Cat#E2650
EnduRen live-cell substrate	Promega	Cat#E6481
Omni-ECL Femto Light Chemiluminescence Kit	EpiZyme	Cat#SQ201
Omni-Easy Instant BCA Protein Assay Kit	Epizyme	Cat#SZJ102
Genejet gel extraction kit	Thermo	Cat#K0692
Deposited data		
<i>E.amu</i> APN-bound RU15-1 RBD cryo-EM structure	This study	EMD-65683, PDB:9W6D

EriCoV S sequence	This study	yan, huan (2025), "Data S1 EriCoV S sequence", Mendeley Data, V1, doi: 10.17632/bj6v2tcv8j.1
<i>E.amu</i> receptor sequences	This study	yan, huan (2025), "Data S2 <i>E.amu</i> receptor sequences", Mendeley Data, V1, doi: 10.17632/87zdkgfvn9.1
94 APN ortholog sequences	This study	yan, huan (2025), "94 APN ortholog sequences", Mendeley Data, V1, doi: 10.17632/sfdtx6fcxj.1
Experimental models: Cell lines		
HEK293T	ATCC	CRL-11268
Caco-2	ATCC	HTB-37
BHK21	ATCC	CCL-10
I1-Hybridoma cell lines	ATCC	CRL-2700
Expi293F	ATCC	A14527
Recombinant DNA		
pVSV-dG-GFP-RU15-1-S	This paper	N/A
pVSV-dG-GFP-IT5-12-S	This paper	N/A
Software and algorithms		
MEGA-X version 10.1.8	Kumar et al.	<a href="https://www.megasoftware.net/">https://www.megasoftware.net/</a>
IQ-TREE	Minh et al.	<a href="http://igtree.cibiv.univie.ac.at/">http://igtree.cibiv.univie.ac.at/</a>
iTOL (v6)	Letunic and Bork	<a href="https://itol.embl.de/">https://itol.embl.de/</a>
UCSF ChimeraX (V.1.7.1)	Goddard et al.	<a href="https://www.rbvi.ucsf.edu/chimerax">https://www.rbvi.ucsf.edu/chimerax</a>
GeoScene Pro (V2.0)	N/A	<a href="https://edutrial.geoscene.cn">https://edutrial.geoscene.cn</a>
PDBePISA	Krissinel and Henrick <sup>91</sup>	<a href="https://www.ebi.ac.uk/pdbe/pisa/pistart.html">https://www.ebi.ac.uk/pdbe/pisa/pistart.html</a>

ClustalW	Thompson et al. <sup>92</sup>	<a href="https://www.genome.jp/tools-bin/clustalw">https://www.genome.jp/tools-bin/clustalw</a>
MAFFT(v7.45071)	Nakamura et al. 2018. <sup>93</sup>	<a href="https://mafft.cbrc.jp">https://mafft.cbrc.jp</a>
Geneious Prime (version 2023.0.4)	Kearse et al. 2012. <sup>94</sup>	<a href="https://www.geneious.com/">https://www.geneious.com/</a>
Other		

## 1 RESOURCE AVAILABILITY

### 2 Lead contact

3 Further information and requests for resources and reagents should be directed to and will be  
4 fulfilled by the lead contact, Huan Yan (严欢) (huanyan@whu.edu.cn)

### 6 Materials availability

7 All plasmids generated in this study are available with a completed Materials Transfer Agreement.  
8 Correspondence and requests for materials can be addressed to the lead contact.

### 10 Data and code availability

- 11 • The density map of the *E.amu* APN–RU15-1 RBD complex has been deposited in the  
12 Electron Microscopy Data Bank under the accession code of EMD-65683. The  
13 corresponding structural coordinate has been deposited in the Protein Data Bank: 9W6D.
- 14 • The 25 EriCoV spike sequences, four receptor sequences from amur hedgehog (*E.amu*  
15 ACE2, *E.amu* DPP4, *E.amu* APN, and *E.amu* TMPRSS2), and 94 APN-coding sequences  
16 have been deposited in Mendeley with DOIs and accession numbers listed in the key  
17 resources table.
- 18 • This paper does not report original code.
- 19 • Any additional information required to reanalyze the data reported in this paper is available  
20 from the lead contact upon request.

## 22 EXPERIMENTAL MODEL AND STUDY PARTICIPANT DETAILS

### 24 Cell lines and culture conditions

25 HEK293T (CRL-3216), Caco-2 (HTB-37), and I1-Hybridoma (CRL-2700) cells were obtained from  
26 the American Type Culture Collection (ATCC). HEK293T and Caco-2 cells were cultured in  
27 Dulbecco's Modified Eagle Medium (DMEM, Monad) supplemented with 10% fetal bovine serum  
28 (FBS; Excell), 1% penicillin-streptomycin (PS; Thermo Fisher Scientific) at 37 °C in a humidified  
29 incubator with 5% CO<sub>2</sub>. The I1-Hybridoma cell line, which produces a neutralizing antibody  
30 against vesicular stomatitis virus glycoprotein (VSV-G), was maintained in Minimum Essential

1 Medium (MEM) with Earle's balanced salts, 2.0 mM L-glutamine (Gibco), and 10% FBS.  
2 HEK293T or Caco-2 stable cell lines overexpressing various receptors were generated using  
3 lentivirus transduction, and then selected and maintained in growth medium with puromycin  
4 (1 µg/mL) or Zeocin (100 µg/mL).

5

#### 6 **Plasma donors**

7 Plasma samples were collected from a random population at Beijing Ditan Hospital, Capital  
8 Medical University. All participants provided written informed consent prior to sample collection.  
9 The study was approved by the Ethics Committee of Beijing Ditan Hospital, Capital Medical  
10 University (Approval No. DTEC-KY2024-112-01). Demographic data for the plasma donors are  
11 presented in [Supplementary Information, Table S3](#).

12

13

#### 14 **METHOD DETAILS**

##### 15 **Receptor sequence retrieval and assembly**

16 The nucleic acid sequences of *E.amu* ACE2, *E.amu* DPP4, *E.amu* APN, and *E.amu* TMPRSS2  
17 were assembled from RNA-seq raw data derived from *Erinaceus amurensis* Kidney (GSA  
18 accession ID: CRX555648) or *Erinaceus amurensis* Lymph (SRA Accession: SRX13651754).  
19 Briefly, raw next-generation sequencing (NGS) reads were downloaded from the Genome  
20 Sequence Archive (GSA) database and Sequence Read Archive (SRA) database and processed  
21 using Cutadapt (v2.4) to remove adapters and discard reads shorter than 30 base pairs. De novo  
22 assembly was performed with MEGAHIT (v1.2.9), using a minimum contig length of 100 bp.  
23 Resulting final contigs were analyzed using Geneious (2023.0.1) and were subjected to Geneious  
24 workflows for mapping reads to the indicated reference sequences under default parameters.

25

##### 26 **Plasmids and vectors**

27 Plasmids for expressing coronavirus receptors or their derivatives were constructed by inserting  
28 human codon-optimized coding sequences obtained through commercial synthesis into the  
29 lentiviral transfer vector (pLVX-EF1a-Puro, Genewiz) with C-terminally fused 3×FLAG tags  
30 (DYKDHD-G-DYKDHD-I-DYKDDDDK).<sup>40</sup> Human TMPRSS2 and *E.amu* TMPRSS2 expressing  
31 plasmid were constructed to pLVX-EF1a-Zeocin (clone based on pLVX-EF1a-Puro with the  
32 resistance gene replaced with Zeocin) with C-terminally fused ALFA-tag (PSRLEEELRRRLTE).<sup>90</sup>  
33 DNA fragments for cloning chimera or mutants were generated by overlap extension PCR or gene  
34 synthesis and verified by commercial DNA sequencing.

35

36 For pseudovirus production, human codon-optimized spike sequences of MO1 (UMO75628.1),  
37 F6 (QGA70692.1), cw\_6 (QQQ34381.1), IT8-1 (QRN68024.1), IT5-19 (QRN68031.1), IT5-17  
38 (QRN68055.1), IT5-1 (QRN68048.1), IT5-11 (QRN68066.1), IT5-12 (QRN68078.1), IT5-15  
39 (QRN68101.1), GER216 (AGX27810.1), GER174 (YP009513010), UK19 (QCC20713.1), PTH9  
40 (XAJ09624.1), RU15-1 (XCN28775.1), RU15-2 (XCN28786.1), PLJ24 (XAJ09723.1), PLJ64  
41 (XAJ09735.1), FR7137 (XNJ65105.1), FR3151 (XNJ65093.1), 229E (OQ920101), were cloned  
42 into the pCAGGS vector with 13-15 C-terminal residues replaced by a HA tag (YPYDVPDYA) to  
43 facilitate S incorporation.<sup>95</sup>

44

1 Plasmids expressing recombinant proteins, including coronavirus antigens, and soluble viral  
2 receptor proteins are described as follows. For CoVs S<sub>1</sub>/RBD-hFc fusion proteins, plasmids were  
3 constructed by inserting S<sub>1</sub> coding sequences from MO1 (residues 18-734), F6 (residues 18-734),  
4 cw\_6 (residues 18-734), IT8-1 (residues 20-735), IT5-19 (residues 20-737), IT5-17 (residues 20-  
5 737), IT5-1 (residues 20-735), IT5-11 (residues 20-740), IT5-12 (residues 20-734), IT5-15  
6 (residues 20-737), GER216 (residues 20-736), GER174 (residues 20-736), UK19 (residues 20-  
7 734), PTH9 (residues 20-736), RU15-1 (residues 20-731), RU15-2 (residues 20-731), PLJ24  
8 (residues 20-735), PLJ64 (residues 20-734), FR7137 (residues 20-731), FR3151 (residues 20-  
9 732); RBD coding sequences from RU15-1 (residues 366-574), MO1 (residues 366-575), PTH9  
10 (residues 367-576), PLJ64 (residues 365-574), GER216 (residues 365-574), 229E (residues 293-  
11 434) into the pCAGGS vector containing an N-terminal CD5 secretion signal peptide  
12 (MPMGSLQPLATLYLLGMLVASVL) and C-terminal hFc-twin-strep-3×FLAG tags  
13 (WSHPQFEKGGGSGGGSSGSAWSHPQFEK-GGGRSDYKDHDGDYKDHDIDYKDDDDK) for  
14 purification and detection. For expressing soluble viral receptor proteins, plasmids were  
15 constructed by inserting ecto-domain coding sequences from *E.amu* APN (residues 60-960),  
16 human APN (residues 66-967) into the pCAGGS vector containing an N-terminal CD5 secretion  
17 signal peptide (MPMGSLQPLATLYLLGMLVASVL) and C-terminal 8×His tags for purification.

18  
19 For Cryo-EM and BLI assays, DNA sequences encoding *E.amu* APN protein (residues 60–960;  
20 GenBank: XP\_007516437.1) and RU15-1 RBD (residues 366–574; GenBank: XCN28775.1)  
21 were obtained from NCBI. An N-terminus CD5 signal peptide and a C-terminus His-tag were  
22 added to both constructs via PCR. These constructs were cloned into the pCAGGS mammalian  
23 expression vectors.

24  
25 Plasmids for human APN gene knockout were constructed by inserting the single-guide RNA  
26 sequence into the pLentiCRISPRv3 vector (clone based on pLentiCRISPRv2-Puro with the  
27 resistance gene replaced with the mCherry coding sequence).

28  
29

### 30 **CRISPR-Cas9 knock-out cell line**

31 Stable Caco-2 cell lines with knockout human aminopeptidase N (APN) were generated via the  
32 CRISPR/Cas9 system. Three guide RNAs (gRNAs) targeting the human APN gene were  
33 designed: gRNA1 (ATCGCCGTGGCCCGCCGCAA), gRNA2 (CGTTCAGGGCATAATCGCCG),  
34 and gRNA3 (CTTCTACCGCAGCGAGTACA). These guided RNAs were cloned into the lentiviral  
35 transfer vector pLVX-mCherry (Genewiz). Lentiviral particles were produced by co-transfecting  
36 HEK293T cells with the gRNA plasmids pMD2.G (Addgene #12259) and the packaging plasmids  
37 psPAX2 (Addgene #12260) at a 2:1:1 ratio using GeneTwin transfection reagent (Biomed,  
38 TG101). Viral supernatant was harvested to transduce Caco-2 cells. Single-cell clones were  
39 isolated by serial dilution at 72 hours post-transduction. APN knockout efficiency was confirmed  
40 by cDNA sequencing, 229E pseudotyped entry assays, and 229E spike protein-mediated cell-cell  
41 fusion assays.

### 42 43 **Protein expression and purification**

44 Proteins for binding, pull-down, or flow cytometry assays were produced in HEK293T cells via  
45 transient transfection, following the manufacturer's guidelines. Supernatants were collected every

1 48 hours post-transfection. Twin-Strep-tagged proteins were enriched using Strep-Tactin XT  
2 4Flow high-capacity resin (IBA, 2-5030-002), washed, and eluted with buffer BXT (100 mM  
3 Tris/HCl, pH 8.0, 150 mM NaCl, 1 mM EDTA, 50 mM biotin). Eluted proteins were concentrated,  
4 buffer-exchanged into PBS by ultrafiltration, aliquoted, and stored at  $-80^{\circ}\text{C}$ .

5  
6 Protein expression and purification were conducted following the established method for Cryo-  
7 EM or BLI analysis.<sup>96,97</sup> Briefly, the plasmids of these proteins were transiently transfected into  
8 suspension-grown HEK293F maintained at  $37^{\circ}\text{C}$  with 8%  $\text{CO}_2$ , rotating at 130 rpm. Supernatants  
9 were harvested 72 hours post-transfection, concentrated, and purified sequentially by Ni-NTA  
10 affinity chromatography and size-exclusion chromatography (SEC) using a Superdex 200  
11 Increase 10/300 GL column (GE Healthcare) equilibrated with PBS buffer.

### 13 **Enzyme-linked immunosorbent assay (ELISA)**

14 ELISA plates were pre-coated with RBD protein from either strain MO1 or RU15-1 at a  
15 concentration of  $1\mu\text{g}/\text{mL}$  in 0.05 M coating buffer (Solarbio, cat. no. C1055) and incubated  
16 overnight at  $4^{\circ}\text{C}$ . After washing, plates were blocked, followed by the addition of 100  $\mu\text{L}$  serially  
17 diluted mouse serum to each well and incubation at room temperature for 30 minutes. Plates were  
18 then washed and incubated with peroxidase-conjugated AffiniPure goat anti-human IgG (H+L)  
19 (Jackson ImmunoResearch, cat. no. 109-035-003) at  $0.25\mu\text{g}/\text{mL}$  for 30 minutes at room  
20 temperature. The reaction was developed using tetramethylbenzidine (TMB) substrate (Solarbio,  
21 cat. no. PR1200) and stopped by the addition of  $\text{H}_2\text{SO}_4$ . Absorbance was measured at 450 nm  
22 using a microplate reader (Thermo Scientific, Multiskan Fc).

### 24 **Animal immunization and antibody screening**

25 All animal experiments were conducted in accordance with protocols approved by the Animal  
26 Welfare Ethics Committee of HFK Biologics (Approval No.: HFK-AP-20250313).

27  
28 Female BALB/c mice aged 6-8 weeks were used in the experiments. Mice were immunized  
29 according to the schedule outlined in Fig. 6A and F. Specifically, mice in the MO1 and RU15-1  
30 RBD protein groups were immunized via subcutaneous injection with 10  $\mu\text{g}$  of purified RBD  
31 protein from either the MO1 strain or RU15-1 strain, each formulated with Freund's adjuvant. The  
32 primary immunization was administered with complete Freund's adjuvant (CFA), followed by a  
33 booster injection formulated with incomplete Freund's adjuvant (IFA) 14 days later. Blood samples  
34 were collected 4 days after the second immunization.

35  
36 Mice in the *E.amu* APN group were immunized via intramuscular injection with 10  $\mu\text{g}$  of *E.amu*  
37 APN mRNA on Day 0, Day 14, and Day 28, followed by a booster injection with 10  $\mu\text{g}$  of purified  
38 *E.amu* APN protein formulated with incomplete Freund's adjuvant (IFA) on Day 35. Blood samples  
39 were collected 4 days after the second immunization and 4 days after the third immunization.  
40 Serum titers were determined using enzyme-linked immunosorbent assay (ELISA).

41  
42 Spleens from euthanized mice were minced in RPMI 1640 medium supplemented with 5% FBS,  
43 filtered through a 100  $\mu\text{m}$  mesh, and treated with  $1 \times$  RBC Lysis Buffer (eBioscience, cat. no. 00-  
44 4333-57). After centrifugation ( $350 \times g$ , 8 min), cells were resuspended in staining buffer (PBS +

1 2% FBS) and adjusted to a final concentration of  $1 \times 10^7$  cells/mL. Recombinant biotinylated RBD  
2 proteins (MO1 or RU15-1 strain) or *E.amu* APN proteins were incubated with streptavidin-  
3 conjugated fluorophores (PE and APC; BioLegend) on ice for at least 30 minutes. Then H<sub>2</sub>O was  
4 added to adjust volume, and the complexes were centrifuged at  $14,000 \times g$  for 10 minutes at 4 °C  
5 to remove aggregates. Before staining, splenocytes were incubated with TruStain FcX™  
6 (BioLegend) for 10 minutes on ice in the dark to block Fc receptors. Antigen probes and  
7 fluorescently conjugated antibodies were then added, and cells were incubated on ice for  
8 30 minutes in the dark. After staining, cells were washed twice with staining buffer ( $400 \times g$ , 5–8  
9 minutes) and resuspended in cold buffer. 7-AAD (eBioscience, cat. no. 00-6993-50) was added  
10 10 minutes before flow cytometry to exclude dead cells. For cell sorting, antigen-specific B cells  
11 were defined as 7-AAD<sup>-</sup>, CD19<sup>+</sup>, IgM<sup>-</sup>/IgD<sup>-</sup>, OVA<sup>-</sup>, and either MO1 RBD<sup>+</sup>, RU15-1 RBD<sup>+</sup>, or  
12 *E.amu* APN<sup>+</sup>, depending on the immunization group. Single B cells were sorted using a MoFlo  
13 Astrios EQ Cell Sorter (Beckman Coulter) directly into 96-well PCR plates.

14  
15 Sorted single B cells were lysed in buffer containing RNase inhibitor, 0.095% Triton X-100, Oligo  
16 dT primer, and dNTPs, followed by cDNA synthesis using the Vazyme R302 kit. Variable regions  
17 of heavy chains and light chains (lambda/kappa) were amplified via two-round PCR. After  
18 verification by 1% agarose gel electrophoresis and magnetic bead purification, the variable region  
19 amplicons were set aside. Separately, the human IgG1 constant region was cloned into pCMV3  
20 vectors using homologous recombination with the ClonExpress II One Step Cloning Kit (Vazyme,  
21 cat. no. C112-02) at 37°C for 30 minutes. Variable regions were recombined into the pCMV3  
22 vectors using the same homologous recombination method. Recombinant plasmids were  
23 transformed into DH5α competent cells (Tsingke, cat. no. TSC-C01), activated at 37°C, and plated  
24 for selection. Recombinant plasmids were transformed into DH5α competent cells (Tsingke, cat.  
25 no. TSC-C01), activated at 37°C, and plated for selection. Plasmid DNA of expanded cultures  
26 was extracted (CW BIO CW2105) after verified by the alignment results of Sanger sequencing.  
27 Protein production was carried out in Expi293F cells. Co-transfection was performed by mixing  
28 the antibody plasmids with polyethylenimine (Yeasen, 40816ES03) in 0.9% NaCl solution before  
29 adding to the cell culture. Cells were maintained under standard culture conditions. After 24 hours,  
30 1 mL of nutrient supplement (OPM Biosciences, F081918-001) was added per culture bottle, with  
31 subsequent feedings every 48 hours during a 6–10 day culturing period. For antibody purification,  
32 supernatant containing the monoclonal antibodies was obtained by centrifugation ( $3,000 \times g$ , 10  
33 minutes). After incubation of Protein A magnetic beads (GenScript, L00695) with the supernatant  
34 for 2 hours, automated purification was achieved by using a KingFisher instrument (Thermo  
35 Fisher). Antibody concentration was measured with a NanoDrop (Thermo Fisher, 840-317400),  
36 while purity was assessed by SDS-PAGE (LabLead, P42015). Screening of monoclonal  
37 antibodies was performed using a pseudovirus neutralization assay. The antibody sequences are  
38 listed in [Supplementary Information, Table S2](#)

39

#### 40 **SPR competitive binding assay**

41 Antibodies were assessed using the Biacore 8K system (GE Healthcare). For competitive  
42 binding experiments, His-tagged MO1 or RU15-1 RBD proteins were immobilized on Anti-His  
43 sensor chips (Cytiva) at a concentration of 1.35 μg/mL for 1 minute. Pairs of antibodies (37.5  
44 μg/mL each) were then sequentially injected over the chip surface, with each injection lasting 2  
45 minutes. The chip surface was regenerated with 1.5 M glycine. Competition between antibodies

1 was quantified using the following score:  $score_{b-a} = 1 - \text{response}_b / \text{response}'_b$  where  $\text{response}_b$   
2 represents the response units (RU) when antibody  $b$  was injected as the second antibody  
3 following antibody  $a$ , and  $\text{response}'_b$  represents the mean RU when antibody  $b$  was injected as  
4 the first antibody.

5

### 6 **Antigen-hFc live-cell binding assay**

7 Live-cell binding assays for coronavirus RBD-hFc fusion proteins were performed as previously  
8 described. HEK293T cells transiently expressing distinct receptors or orthologous APNs were  
9 incubated 48 hours post-transfection with recombinant RBD-hFc proteins (2  $\mu\text{g}/\text{mL}$  diluted in  
10 DMEM) for 30 minutes at 37°C (5%  $\text{CO}_2$ ). Cells were gently washed once with Hanks' Balanced  
11 Salt Solution (HBSS), then stained for 1 hour at 37°C with Alexa Fluor 488-conjugated goat anti-  
12 human IgG (1  $\mu\text{g}/\text{mL}$ ; Thermo Fisher Scientific, #A11013) and Hoechst 33342 nuclear  
13 counterstain (1:10,000 dilution in HBSS). Both reagents were prepared in HBSS containing 1%  
14 bovine serum albumin (BSA). After staining, cells were washed twice with HBSS and imaged with  
15 fresh HBSS. Fluorescence microscopy used an MI52-N system (Nikon). Relative fluorescence  
16 intensities (RFU) were quantified using a Varioskan LUX multimode plate reader (Thermo  
17 Scientific).

18

19 For experiments with RBD-specific antibody competition, recombinant RBD-hFc proteins (2  
20  $\mu\text{g}/\text{mL}$ ) and indicated RBD-specific antibodies (10  $\mu\text{g}/\text{mL}$ ) were mixed within 50  $\mu\text{L}$  DMEM for 1  
21 hour at 37°C and then applied to HEK293T cells transiently expressing *E.amu* APN for RBD-hFc  
22 binding efficiency evaluation.

23

### 24 **Flow cytometry**

25 To analyze RBD-hFc binding by flow cytometry, HEK293T cells transiently expressing the  
26 indicated APN orthologs were detached with 5 mM EDTA/PBS 24 hours post-transfection. Cells  
27 were incubated with RU15-1 or MO1 RBD-hFc proteins (2  $\mu\text{g}/\text{mL}$ ) at 4°C for 1 hour. After two  
28 PBS washes, cells were stained for 1 hour at 4°C using Alexa Fluor 488- or DyLight 594-  
29 conjugated goat anti-human IgG antibodies to detect RBD binding (Thermo Fisher Scientific;  
30 A11013). Following two additional PBS washes, 20,000 live cells (gated based on SSC/FSC)  
31 were analyzed on a CytoFLEX flow cytometer (Beckman).

32

### 33 **Western blot**

34 Western blotting was performed to assess S glycoprotein incorporation into VSV pseudoviruses.  
35 Pseudovirus-containing supernatants were concentrated through a 30% sucrose cushion (30%  
36 sucrose, 15 mM Tris-HCl, 100 mM NaCl, 0.5 mM EDTA) by centrifugation at 20,000  $\times g$  for 1 hour  
37 at 4°C. Pellets were resuspended in 1  $\times$  SDS loading buffer, boiled at 95°C for 30 minutes, and  
38 subjected to SDS-PAGE and immunoblotting.

39

40 To evaluate expression of different APN orthologs, HEK293T cells were transfected for 24 hours,  
41 lysed in 1% Triton X-100 at 4°C for 10 minutes, and clarified by centrifugation at 12,000  $\times g$  for 5  
42 minutes. Supernatants were mixed with 5  $\times$  loading buffer and analyzed by Western blot.  
43 Membranes were blocked with 5% milk in PBST for 1 hour at room temperature, incubated  
44 overnight at 4°C with anti-HA or anti-APN polyclonal antibodies (Abclonal), and then probed with  
45 goat anti-mouse IgG secondary antibody for 1 hour at room temperature. After four washes in

1 PBST, signals were visualized using the Omni-ECL Femto Light Chemiluminescence Kit  
2 (EpiZyme, SQ201) and imaged on a ChemiDoc MP system (Bio-Rad).

### 4 **Immunofluorescence assay**

5 Immunofluorescence assays were performed to assess the expression levels of APN orthologs  
6 with C-terminal fused 3×FLAG tags. Cells expressing the receptors were seeded in the 96-well  
7 plates. Specifically, the transfected cells were fixed and permeabilized with 100% methanol for  
8 10 minutes at room temperature. Then the cells were incubated with a mouse antibody M2  
9 (Sigma-Aldrich, F1804) diluted in HBSS/1% BSA for 1 hour at 37 °C. After one HBSS wash, the  
10 cells were incubated with Alexa Fluor 594-conjugated goat anti-mouse IgG (Thermo Fisher  
11 Scientific, A32742) secondary antibody diluted in 1% BSA/PBS for one hour at 37 °C. The images  
12 were captured with a fluorescence microscope (Mshot, MI52-N) after the nucleus was stained  
13 blue with Hoechst 33342 reagent (1:2,000 dilution in HBSS).

### 15 **Pull-down assay**

16 For pull-down assays, recombinant viral RBD-hFc-Strep-FLAG and soluble *E.amu* APN-His  
17 proteins were expressed in eukaryotic cells and purified by affinity chromatography. Viral RBD-  
18 hFc-Strep-FLAG protein (1 µg/mL) was incubated with 30 µL suspended Mag-Strep beads in 500  
19 µL PBS at 4 °C for 1 hour. Beads were washed three times with cold PBS and then incubated with  
20 2 µg of *E.amu* APN-His protein in 1 mL PBS at 4 °C for an additional hour. After washing three  
21 times with cold PBS, beads were resuspended in PBS, denatured in 1 × SDS-loading buffer, and  
22 boiled for 20 minutes. Samples were analyzed by SDS-PAGE followed by western blotting.

### 24 **Biolayer interferometry (BLI) binding assay**

25 Binding affinities were measured using bio-layer interferometry (BLI) on an Octet RED96  
26 instrument (Molecular Devices), following a protocol similar to that described above.<sup>98,99</sup> Briefly,  
27 recombinant MO1 and RU15-1 RBD-His proteins (50 µg/mL) were immobilized onto Ni-NTA  
28 biosensors (ForteBio) for 300 s. Following loading, the biosensors were transferred to kinetics  
29 buffer (PBS supplemented with 0.02% Tween-20; PBST) for 60 s to remove unbound proteins.  
30 The sensors were then immersed in PBST containing serial dilutions (0–10 µM) of soluble *E.*  
31 *amurensis* APN ectodomain (twin-Strep-tag) for 120 s to monitor the association phase, followed  
32 by a 120 s dissociation phase in PBST. Data acquisition and analysis were performed using Octet  
33 Acquisition 9.0 and Octet Analysis 9.0 software (ForteBio), respectively.

### 35 **Cell-cell fusion assays**

36 A cell-cell fusion assay based on dual-split proteins (DSPs) was performed in HEK293T or Caco-  
37 2 cells stably expressing *E.amu* APN. Two groups of cells were prepared to assess the S  
38 glycoprotein-mediated membrane fusion promoted by receptor interaction. Group A cells were  
39 transfected with plasmids expressing S glycoprotein and rLucN(1-155)-sfGFP1-7(1-157), while  
40 group B cells received plasmids encoding the S glycoprotein and sfGFP8–11(158–231)-  
41 rLuc(156–311). At 12 hours post-transfection, both groups of cells were trypsinized, mixed, and  
42 seeded into a 96-well plate at  $8 \times 10^4$  cells per well. At 24 h post-transfection, the cells were  
43 washed twice with DMEM and then incubated with DMEM containing the indicated concentrations  
44 of Trypsin, from porcine pancreas (Sigma-Aldrich, T4549) for 30 minutes at 37 °C. Trypsin activity  
45 was then quenched by replacing the medium with DMEM supplemented with 10% FBS and

1 Hoechst 33342 (1:5,000) for nuclear staining. Syncytia formation with green fluorescence was  
2 assessed after 1.5 hours post-trypsin treatment, and images were captured either by a  
3 fluorescence microscope (MI52-N; Mshot) or an ELISPOT reader (S6 UNIVERSAL M2).

#### 4 5 **Pseudovirus production**

6 Pseudoviruses carrying coronavirus S glycoproteins were generated using a vesicular stomatitis  
7 virus (VSV)-based pseudotyping system based on a previously published protocol with minor  
8 modifications.<sup>50</sup> Briefly, HEK293T cells were transfected with plasmids encoding the S proteins  
9 using Lipofectamine 2000 (Biosharp, China). After 24 hours, the cells were infected with VSV-  
10  $\Delta$ G-fLuc-GFP ( $1 \times 10^6$  TCID<sub>50</sub>/mL) in DMEM supplemented with 8  $\mu$ g/mL polybrene and  
11 incubated for 2 hours at 37 °C on a shaker. The inoculum was then replaced with fresh DMEM or  
12 SMM 293-TII Expression Medium (Sino Biological, M293TII) containing an anti-VSV-G  
13 monoclonal antibody (I1, 1  $\mu$ g/mL) to neutralize residual input virus. After another 24 hours, the  
14 supernatant containing pseudoviruses was harvested, clarified by centrifugation at  $13,523 \times g$  for  
15 5 minutes at 4 °C, and stored at -80 °C until use.

#### 16 17 **Single-round pseudovirus entry and neutralization assay**

18 Single-round EriCoV pseudovirus entry assays were performed in HEK293T or Caco-2 cells  
19 transiently or stably expressing various receptors. Cells were seeded in 96-well plates at  $3 \times 10^4$   
20 cells/well and infected with pseudoviruses ( $1.5 \times 10^5$  TCID<sub>50</sub> in 100  $\mu$ L) in the presence of the I1  
21 anti-VSV-G neutralizing antibody to minimize background.

22  
23 For proteolytic activation, pseudoviruses were pretreated with 1.25 mg/mL trypsin (Sigma-Aldrich,  
24 T4549) for 1 hour at 37°C. In experiments shown in Figures 2B–C, 2J, 3D, and 5D, trypsin activity  
25 was quenched with 10% FBS. In experiments for Figure 2G (RU15-1 only) 125  $\mu$ g/mL trypsin was  
26 maintained during inoculation in serum-free DMEM. For untreated controls, PBS was added  
27 instead. At 16–20 hours post-infection (hpi), intracellular luciferase activity was measured using  
28 the Bright-Glo Luciferase Assay System (Promega, E2620) on a Thermo Varioskan LUX, or  
29 GloMax 20/20 Luminometer (Promega).

30  
31 Monoclonal antibodies or plasma samples were serially diluted in DMEM (Hyclone, cat. no.  
32 SH30243.01) and incubated with pseudovirus in 96-well plates at 37°C under 5% CO<sub>2</sub> for 1 hour.  
33 Trypsin-digested HEK293T-*E.amu* APN cells were then seeded into the plates and cultured for  
34 24 hours. After discarding half of the supernatant, reconstituted lyophilized Bright-Lite Luciferase  
35 Assay Substrate was mixed with Bright-Lite Luciferase Assay Buffer (Vazyme, cat. no. DD1209-  
36 03-AB) before being added to the wells for incubation in the dark. Luminescence intensity was  
37 measured using a microplate spectrophotometer (PerkinElmer, model HH3400). The 50%  
38 inhibitory concentration (IC<sub>50</sub>) and the 50% neutralization titer (NT50) were calculated via four-  
39 parameter logistic regression using PRISM software (version 9.0.1).

#### 40 41 **rcVSV-CoV amplification and neutralization assay**

42 Experiments involving replication-competent VSV-S (rcVSV-S) were approved by the Biosafety  
43 Committee of the State Key Laboratory of Virology and Biosafety of Wuhan University and  
44 performed under Biosafety Level 2 (BSL-2) conditions. Plasmids for rescuing rcVSV-S expressing  
45 IT5-12 or RU15-1 spike (S) glycoproteins were constructed by substituting the firefly luciferase

1 (fLuc) coding sequence with coronavirus S gene sequences in the pVSV-ΔG-fLuc-GFP vector  
2 backbone.<sup>66,87</sup> In these recombinant viruses, the VSV-G gene was replaced with genomically  
3 encoded S glycoproteins, with a GFP reporter expression cassette for visualization. rcVSVs  
4 expressing IT5-12 or RU15-1 S glycoproteins were generated via reverse genetics following a  
5 modified published protocol. Briefly, BHK21 cells seeded at 80% confluence in 6-well plates were  
6 infected with recombinant vaccinia virus expressing T7 RNA polymerase (vvT7 provided by  
7 Mingzhou Chen's laboratory, Hubei University) at a multiplicity of infection (MOI) of 5 for 45  
8 minutes at 37°C. Following infection, cells were transfected with pVSV-ΔG-GFP-S plasmids and  
9 helper plasmids (mass ratio: 5:3:5:8:1 for pVSV-ΔG-GFP-S:pBS-N:pBS-P:pBS-G:pBS-L).  
10 Supernatants containing rcVSV-S (designated P0) were harvested 48 hours post-transfection,  
11 filtered (0.22 μm) to eliminate residual vvT7, and used to infect Caco-2 cells pre-transfected with  
12 VSV-G for production of passage 1 (P1) viruses. To generate passage 2 (P2) viral particles  
13 carrying IT5-12 or RU15-1 S glycoproteins, P1 viruses were used to infect Caco-2 cells stably  
14 expressing *E.amu* APN without ectopic VSV-G expression and in the presence of anti-VSV-G (I1-  
15 hybridoma supernatant).

16  
17 For viral amplification assays,  $3 \times 10^4$  trypsinized Caco-2 cells expressing relevant APNs were  
18 seeded in 96-well plates and incubated with rcVSV-CoV ( $1 \times 10^4$  TCID<sub>50</sub>/100 μL) in DMEM  
19 supplemented with 2% FBS, with or without TPCK-treated trypsin. Nuclei were stained with  
20 Hoechst 33342 (1:10,000 dilution in HBSS) for 30 minutes at 37°C. Fluorescence images were  
21 acquired at designated time points post-infection using an MI52-N fluorescence microscope  
22 (Nikon).

23  
24 For antibody neutralization assays, *E.amu* APN-expressing Caco-2 cells were seeded in 96-well  
25 plates at a density of  $5 \times 10^4$  cells per well. Twelve hours later, rcVSV-CoV was incubated with  
26 the indicated concentrations of antibodies in DMEM for 1 hour at 37 °C, then added to the target  
27 cells in DMEM containing 2 % FBS. At the indicated time post-infection, nuclei were stained with  
28 Hoechst 33342 (1:10,000 dilution in HBSS) for 30 minutes at 37 °C, and fluorescence images  
29 were acquired using a fluorescence microscope (MI52-N).

30  
31

### 32 **Cryo-EM sample preparation and data collection**

33 Cryo-EM samples were prepared by mixing the respective protein components—either *E.amu*  
34 APN, RU15-1 RBD—at 1:3 molar ratios, followed by a brief incubation at 4°C overnight, similar to  
35 the previous frozen sample preparation.<sup>100</sup> Each complex was subjected to size-exclusion  
36 chromatography (SEC) to ensure sample homogeneity. The samples were applied to glow-  
37 discharged holey carbon-coated gold grids (C-flat, 300 mesh, 1.2/1.3, Protochips Inc.), blotted for  
38 7 seconds without blotting force under 100% relative humidity, and plunge-frozen in liquid ethane  
39 using a Vitrobot (FEI).

40 Cryo-EM data were collected on an FEI Titan Krios transmission electron microscope operated  
41 at 300 kV. Movies were recorded using a K3 Summit direct electron detector in counting mode,  
42 with each movie consisting of 32 frames (0.2 s per frame) and a total electron dose of  $60 \text{ e}^-/\text{Å}^2$ .  
43 Automated data acquisition was performed using SerialEM. For the *E.amu* APN–RU15-1 RBD  
44 complex, data were acquired at a nominal magnification of 29,000 ×, corresponding to a calibrated  
45 pixel size of 0.83 Å. The defocus range was set between  $-1.2$  and  $-2.0$  μm.

1  
2  
3  
4  
5  
6  
7  
8  
9  
10  
11  
12  
13  
14  
15  
16  
17  
18  
19  
20  
21  
22  
23  
24  
25  
26  
27  
28  
29  
30  
31  
32  
33  
34  
35  
36  
37  
38  
39  
40  
41  
42  
43  
44  
45

## Cryo-EM data processing, model fitting, and refinement

A total of 10,621 micrographs were collected for the *E.amu* APN–RU15-1 RBD complex. Beam-induced motion correction was performed using MotionCor2, and the defocus values of each micrograph were estimated with Gctf.<sup>101</sup> A total of 3,191,475 particles were automatically picked and extracted for reference-free 2D classification using cryoSPARC.<sup>102</sup> Based on the 2D class averages, 1,548,480 particles were selected for ab initio reconstruction in cryoSPARC with no symmetry imposed, resulting in multiple initial models representing potential conformational states of the complex.

The best candidate model was then selected and subjected to non-uniform refinement in cryoSPARC to generate the final cryo-EM density maps. The final resolution of each structure was estimated using the gold-standard Fourier shell correlation (FSC) criterion (threshold = 0.143), and local resolution was evaluated using ResMap.<sup>103</sup> A detailed summary of the image processing workflow is provided in [Supplementary Information, Figure S4A](#), and the statistics are listed in [Supplementary Information, Table S1](#).

The atomic model of *E.amu* APN–RU15-1 RBD complex was generated by fitting *E.amu* APN and RU15-1 (predicted by AlphaFold3) into the cryo-EM densities described above by Chimera,<sup>104</sup> followed by manual adjustment and correction according to the protein sequences and densities in Coot,<sup>105</sup> as well as real space refinement using Phenix.<sup>106</sup> Details of the refinement statistics of the complexes are summarized in [Supplementary Information, Table S1](#).

## Bioinformatic and structural analysis

A dataset of 25 unique EriCoV S glycoproteins was gathered via BLAST searches of the NCBI database using the HKU31-F6 S protein as a reference sequence. After eliminating redundant sequences with 100% RBD amino acid identity and those containing ambiguous base calls, 22 unique RBD sequences were collected for further analysis. The RBD and S protein sequences used for phylogenetic analysis in Figure 1C and Figure S1B were aligned via MAFFT-DASH, while the RBM sequence alignments in Figure 1F were aligned via MAFFT (v7.45071) with manual adjustments to optimize indel positioning. Phylogenetic trees were constructed using IQ-TREE (version 2.0.6) under the Maximum Likelihood model with 1,000 bootstrap replicates. Evolutionary model selection was performed using ModelFinder Plus in IQ-TREE with Bayesian Information Criterion (BIC) optimization. The best-fit models implemented were: WAG+G4 model for RBDs, GTR+F+I+R4 model for the whole genomes, WAG+F+I+R3 model for spike proteins, and Q.plant+F+I+R6 model for the APN protein sequences. Pairwise sequence identities were calculated in Geneious Prime (version 2023.0.4) (<https://www.geneious.com/>) following MAFFT-DASH alignment. Experimentally resolved structures used for structural analysis in this study included: MERS-CoV RBD (4KQZ), HKU4-1 RBD (4QZV), HKU5-19s RBD (9D32), NeoCoV RBD (PDB: 7WPO), EriCoV-GER216 RBD (9JMG), MOW15-22 RBD (9C6O), HCoV-229E RBD-hAPN complex (6U7E), PDCoV RBD-pAPN complex (7VPQ), and PRCV RBD-pAPN complex (4F5C). Structural visualization and analysis were performed using ChimeraX (v1.7.1). A total of 94 orthologous APN protein sequences from mammals and *Gallus gallus* were collected from NCBI (either directly annotated or extracted from whole-genome assemblies) and UniProt. Multiple sequence alignment was performed using MAFFT (v7.45071),<sup>93</sup> and phylogenetic trees were

1 constructed with IQ-TREE using the Maximum Likelihood method with 1,000 bootstrap  
2 replicates.<sup>107</sup> The resulting trees were visualized using iTOL (<https://itol.embl.de/>).

3

#### 4 **QUANTIFICATION AND STATISTICAL ANALYSIS**

5 Most experiments related to pseudovirus infection were conducted 2-3 times with 2-3 biological  
6 repeats; technical repeats are indicated in the legends. Representative results were shown. All  
7 data were presented by MEAN or MEAN  $\pm$  SD. Unpaired two-tailed t-tests were conducted for all  
8 statistical analyses for two independent groups using GraphPad Prism 10.  $P < 0.05$  was  
9 considered significant. \*:  $P < 0.05$ , \*\*:  $P < 0.01$ , \*\*\*:  $P < 0.005$ , and \*\*\*\*:  $P < 0.001$ , NS: not significant.  
10 No data were excluded for data analysis.

11

1 Supplementary information for

2

3 **Convergent utilization of APN receptor by hedgehog merbecoviruses**

4 Peng Liu<sup>1,7</sup>, Qianhui Zhu<sup>2,3,7</sup>, Jingyi Liu<sup>4,7</sup>, Zhixing Ma<sup>1,7</sup>, Yuanling Yu<sup>5</sup>, Chen Liu<sup>1</sup>, Chengbao Ma<sup>1</sup>,  
5 Junyu Si<sup>1</sup>, Xiao Yang<sup>1</sup>, Meiling Huang<sup>1</sup>, Yehui Sun<sup>1</sup>, Xiao Yu<sup>1</sup>, Yucheng Sun<sup>1</sup>, Tianci Liu<sup>2,3</sup>,  
6 Lingling Yu<sup>5</sup>, Qianran Wang<sup>5</sup>, Yunlong Cao<sup>4,5,6,\*</sup>, Xiangxi Wang<sup>2,3,\*</sup>, Huan Yan<sup>1,8,\*</sup>

7

8 **The PDF document file includes:**

9

10 Figure S1 to S6 and Table S1

11 Excel file for Table S2

12 Excel file for Table S3

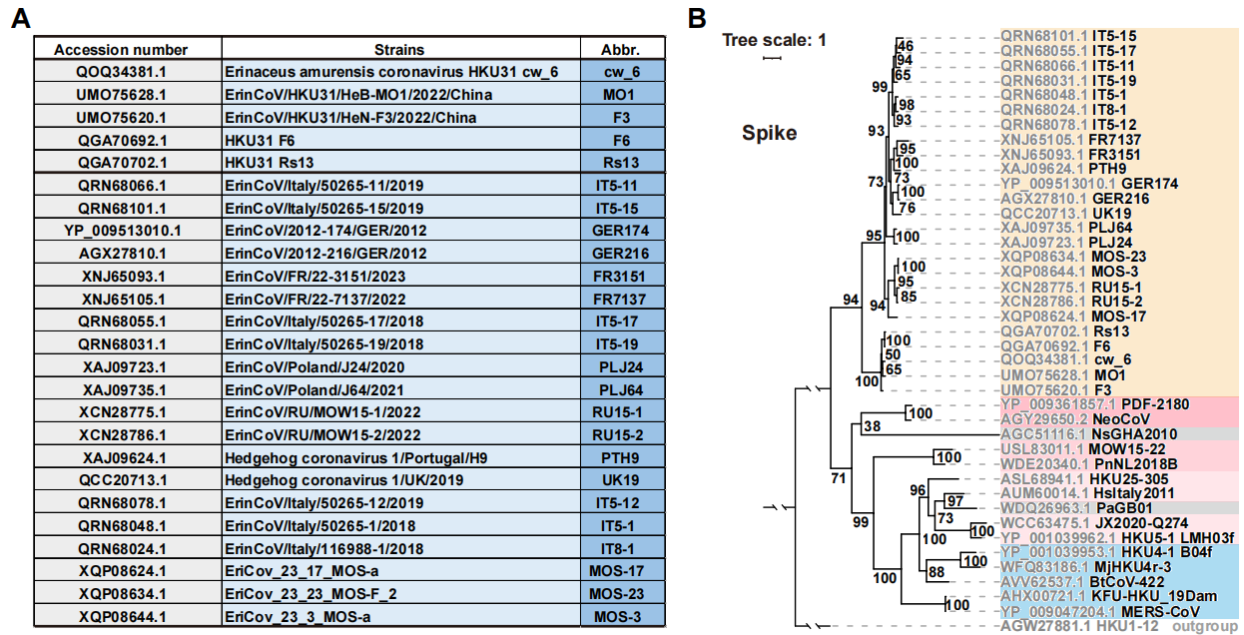
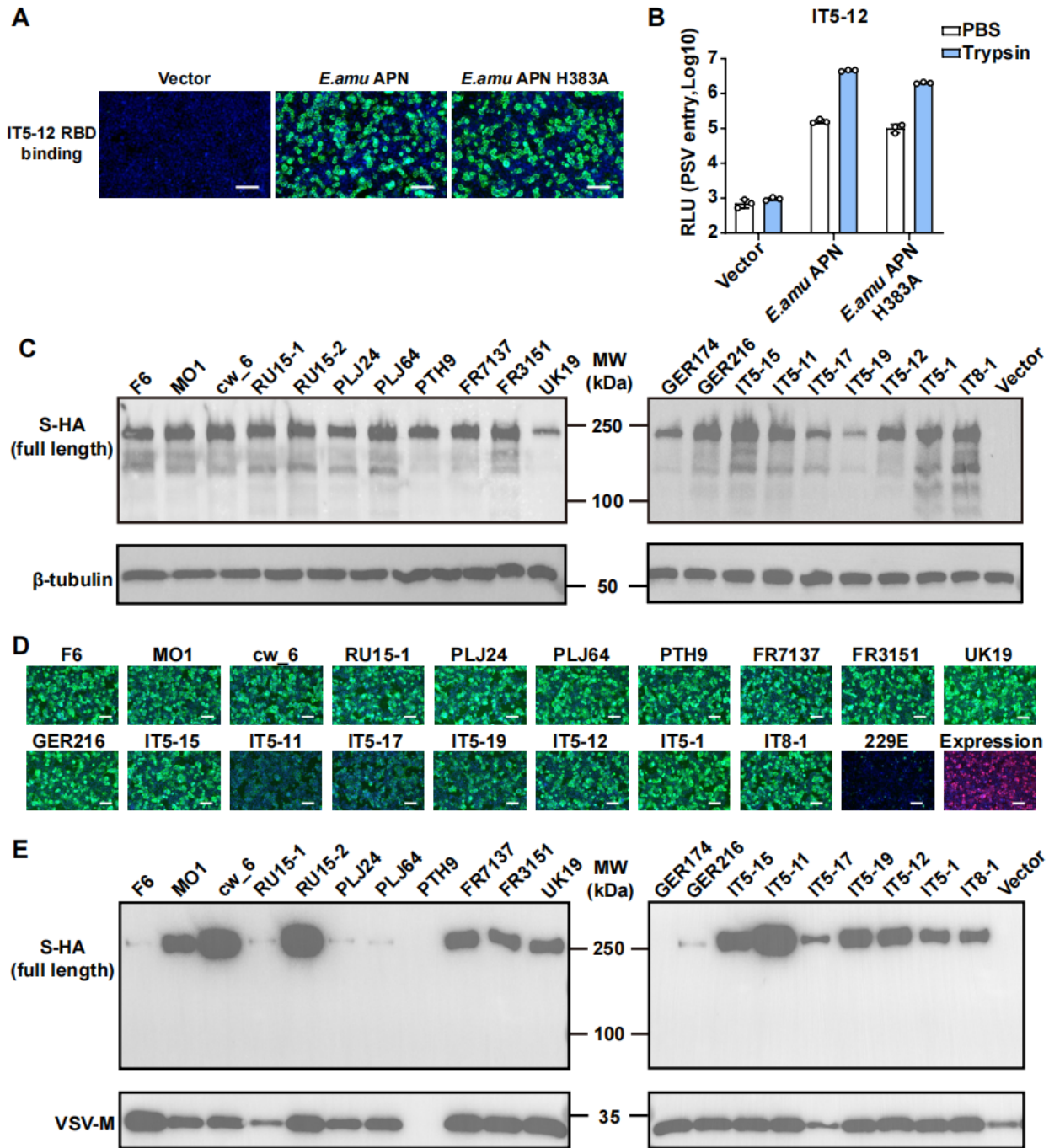


**Figure S1 Abbreviations and phylogenetic analysis of EriCoV S glycoprotein sequences.**

(A) The accession number and abbreviation of the EriCoV strain names involved in this study.

(B) Phylogenetic trees based on amino acid sequences of S glycoproteins from selected representative merbecoviruses were generated using IQ-TREE. Outgroup: HKU1-12.

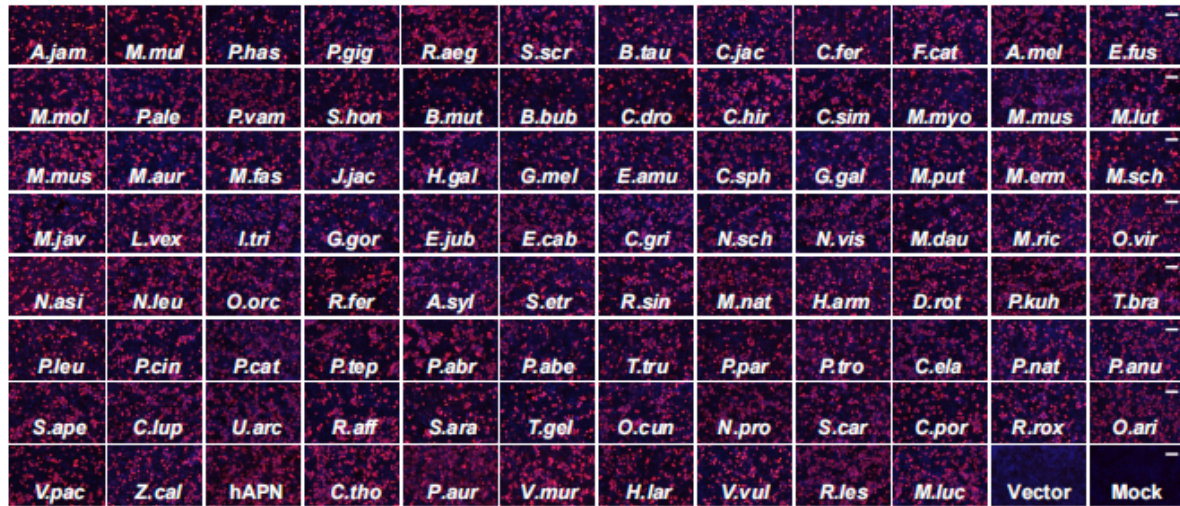
1  
2  
3  
4  
5  
6



1  
2 **Figure S2 | *E.amu* APN is utilized by various EriCoV strains in a catalytic activity-**  
3 **independent manner. (A-B) *E.amu* APN receptor function is independent of its catalytic activity.**  
4 IT5-12 RBD-hFc binding (A) and pseudovirus entry (B) in HEK293T cells transiently expressing  
5 WT *E.amu* APN or *E.amu* APN with H383A catalytic site mutation. Pseudoviruses were pretreated  
6 with 1.25 mg/mL trypsin. Mean  $\pm$  SD for n=3 biological replicates. (C) Western blot analysis of  
7 indicated EriCoV S protein expression in HEK293T cells.  $\beta$ -tubulin served as a loading control.  
8 (D) EriCoV RBD-hFc binding in HEK293T cells transiently expressing *E.amu* APN, with 229E  
9 RBD as a negative control. (E) Detection of EriCoV S glycoprotein in VSV pseudovirions via  
10 Western blot using an anti-HA antibody targeting the C-terminally fused HA tag. VSV-M serves  
11 as a loading control. Scale bars: 100  $\mu$ m for panels A and D.

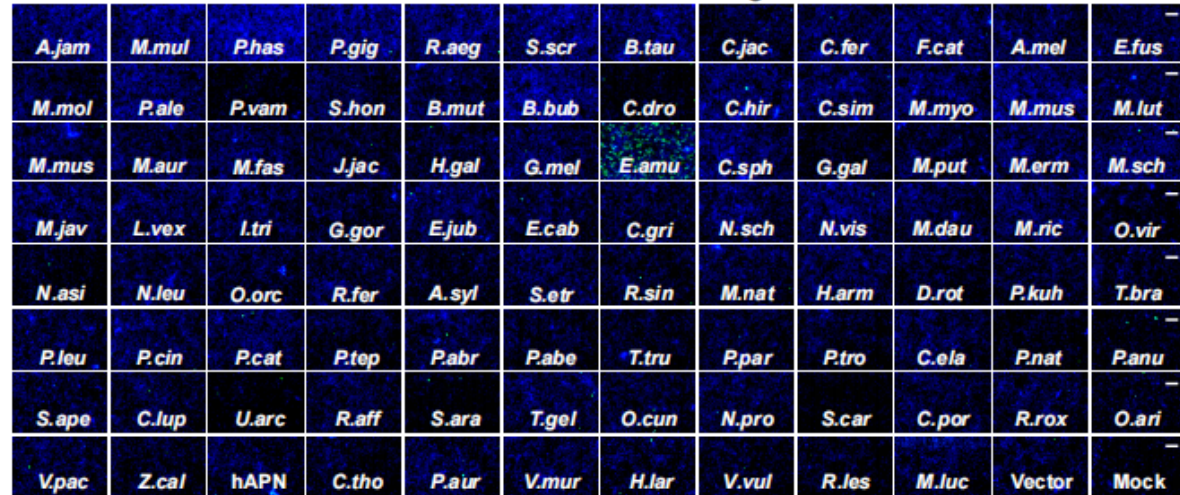
**A**

**Expression of APN orthologs (FLAG)**

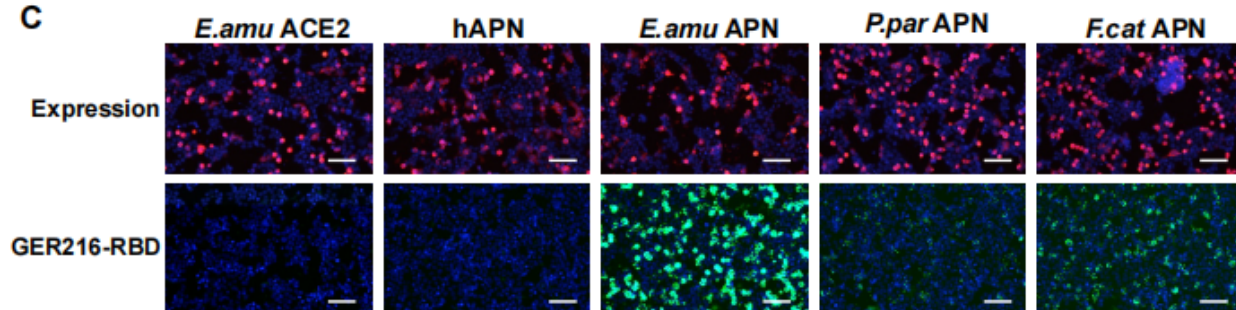


**B**

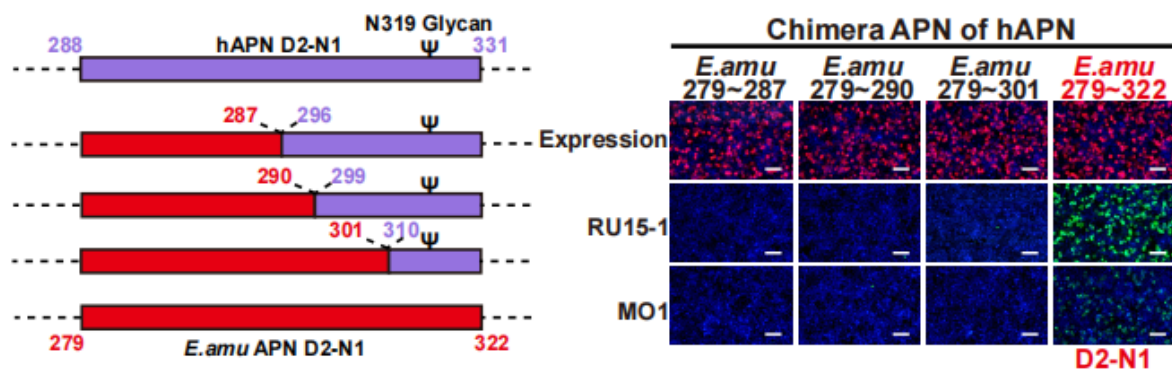
**MO1 RBD-hFc binding**



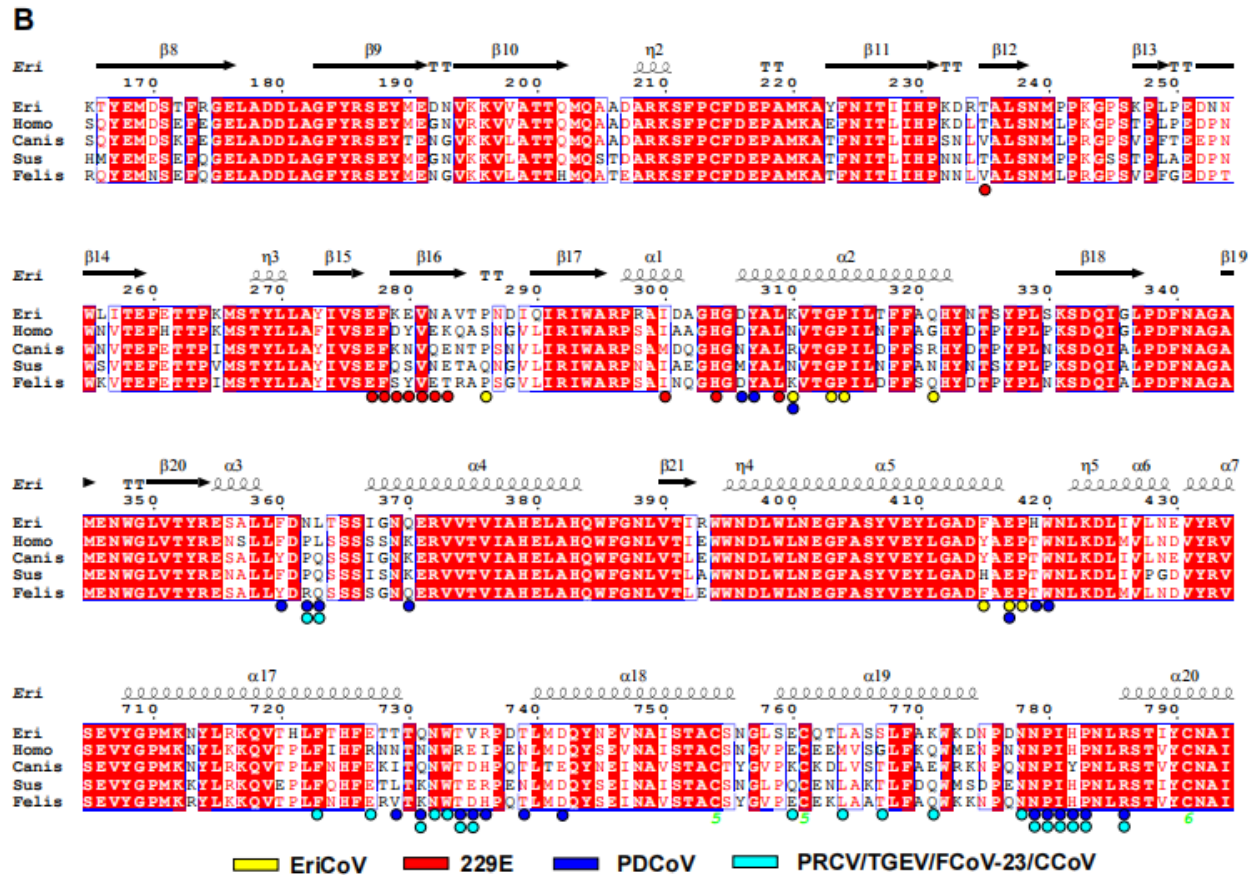
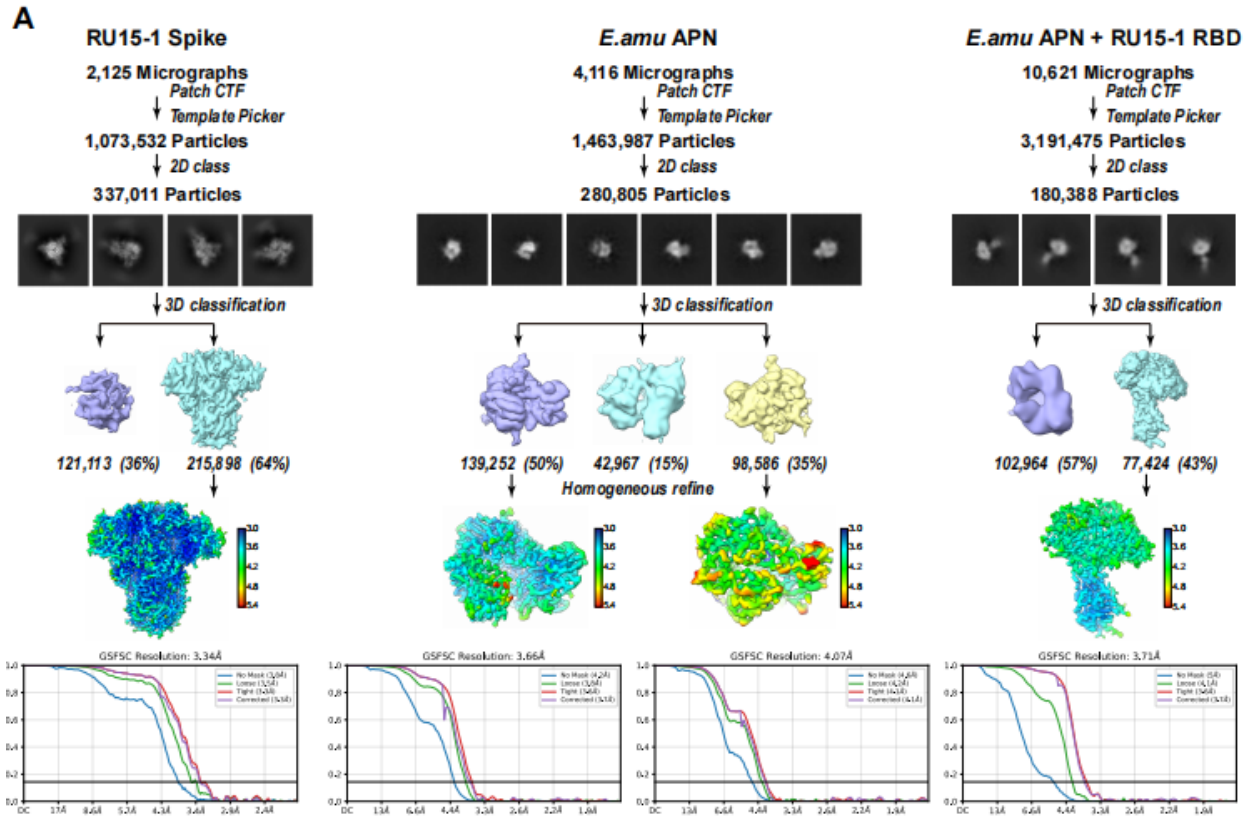
**C**



**D**



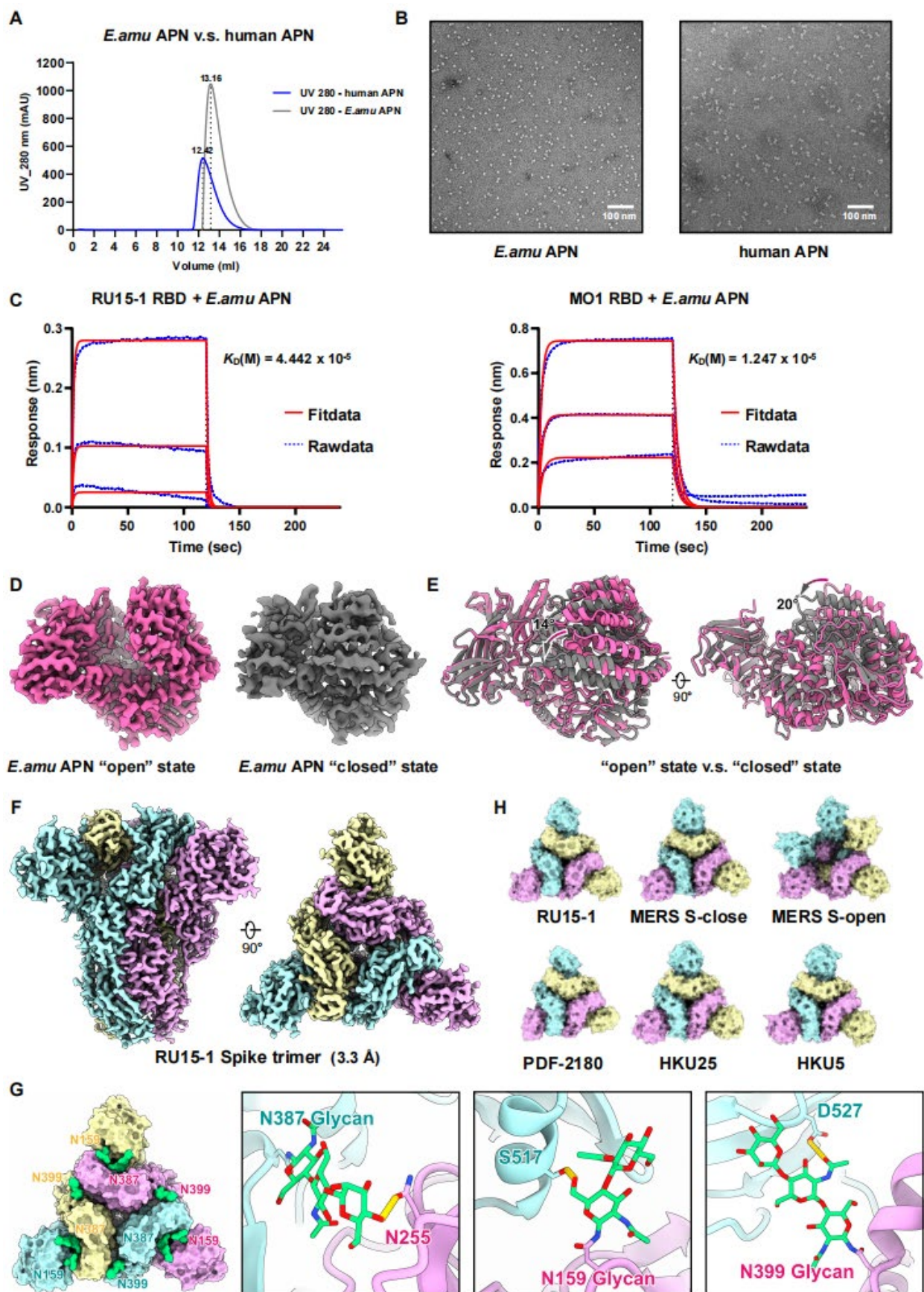
1 **Figure S3 | APN tropism and host range determinant of EriCoV.** (A) Expression of 94 APN  
2 orthologs in HEK293T cells transiently transfected with C-terminally fused 3×FLAG tags was  
3 examined through immunofluorescence (red). (B) Binding of MO1 S<sub>1</sub>-hFc (green) to HEK293T  
4 cells transiently expressing the indicated APN orthologs, assessed by immunofluorescence using  
5 an anti-hFc antibody (green). (C) GER216 RBD-hFc binding (green) to HEK293T cells transiently  
6 expressing the indicated APN orthologs (red). (D) Substitution of the full D2-N1 region (residues  
7 279-322) from *E.amu* APN is required for hAPN to support RBD-hFc binding of RU15-1 and MO1.  
8 N-319 glycosylation in hAPN is labeled with Ψ. Scale bars: 100 μm for panels A, B, C, and D.  
9



1

1 **Figure S4 | Cryo-EM data processing workflow and binding site analysis.** (A) Flowcharts for  
2 structure determinations of the RU15-1 Spike, *E.amu* APN, and RU15-1 RBD–*E.amu* APN  
3 complex. Gold-standard Fourier shell correlation (FSC) curves are shown to assess map quality  
4 and resolution. Local resolution assessments of cryo-EM maps using rainbow are shown. (B)  
5 Multiple sequence alignment of APN orthologs from different species. APN sequences from  
6 *Erinaceus amurensis* (Eri), *Homo sapiens* (Homo), *Canis lupus* (Canis), *Sus scrofa* (Sus), and  
7 *Felis catus* (Felis) are aligned to highlight sequence conservation and variability. Binding sites  
8 located within 4 Å of viral RBDs are indicated by colored circles: yellow for EriCoV, red for HCoV-  
9 229E, blue for PDCoV, and cyan for PRCV, TGEV, FCoV-23, and CCoV, which share a common  
10 APN-binding mode.

11  
12  
13  
14



1

1 **Figure S5 | Conformations of *E.amu* APN, structural features of the RU15-1 spike and BLI**  
2 **assay. (A)** Size-exclusion chromatography profiles of recombinant *E.amu* and human APN.  
3 Recombinant *E.amu* APN and human APN were expressed and purified using a Superdex 200  
4 size-exclusion chromatography column. The elution profiles of size-exclusion chromatography  
5 traces are shown, with *E.amu* APN represented by the blue trace and human APN by the gray  
6 trace. **(B)** Negative-stain EM micrographs of *E.amu* APN (left) and human APN (right). **(C)** BLI  
7 assays analyzing the binding kinetics of *E.amu* APN ectodomains to immobilized monomeric  
8 RU15-1 RBD and MO1 RBD-His proteins on Ni-NTA biosensors. The BLI assay was performed  
9 using a 1:1 binding model with fixed-phase and mobile-phase interactions. Data were analyzed  
10 by global fitting, and the equilibrium dissociation constant ( $K_D$ ) was derived from the ratio of the  
11 association rate ( $k_a$ ) to the dissociation rate ( $k_d$ ). The fits are shown as red lines. **(D)**  
12 Conformational states of *E.amu* APN monomer. Cryo-EM structures of *E.amu* APN in the open  
13 (pink, PDB: 9ZA1) and closed (gray, PDB: 9ZA2) conformations are shown (left). **(E)** Structural  
14 superposition of the two conformations reveals a  $\sim 14^\circ$  angular displacement (middle left). Upon  
15 a  $90^\circ$  rotation, a larger deviation of  $\sim 20^\circ$  is observed between the open and closed states (middle  
16 right and right). **(F)** Cryo-EM structure of the RU15-1 spike trimer. Cryo-EM reconstruction of the  
17 RU15-1 spike trimer at 3.3 Å resolution shown in front (left) and top (right) views. The three  
18 protomers are colored cyan, purple, and yellow, respectively. **(G)** Structural representation of  
19 glycosylation sites on the RU15-1 Spike. N-linked glycosylation sites are shown in green (left:  
20 cartoon representation; right: stick representation). The three protomers are depicted in cyan,  
21 purple, and yellow, respectively, and key residues are annotated. **(H)** Cryo-EM reconstructions  
22 showing the conformational states of spike trimers from representative merbecoviruses, including  
23 RU15-1, MERS-CoV (open and close), PDF-2180, HKU25, and HKU5. The three protomers are  
24 colored cyan, purple, and yellow, respectively.

25  
26  
27  
28  
29  
30  
31  
32  
33  
34

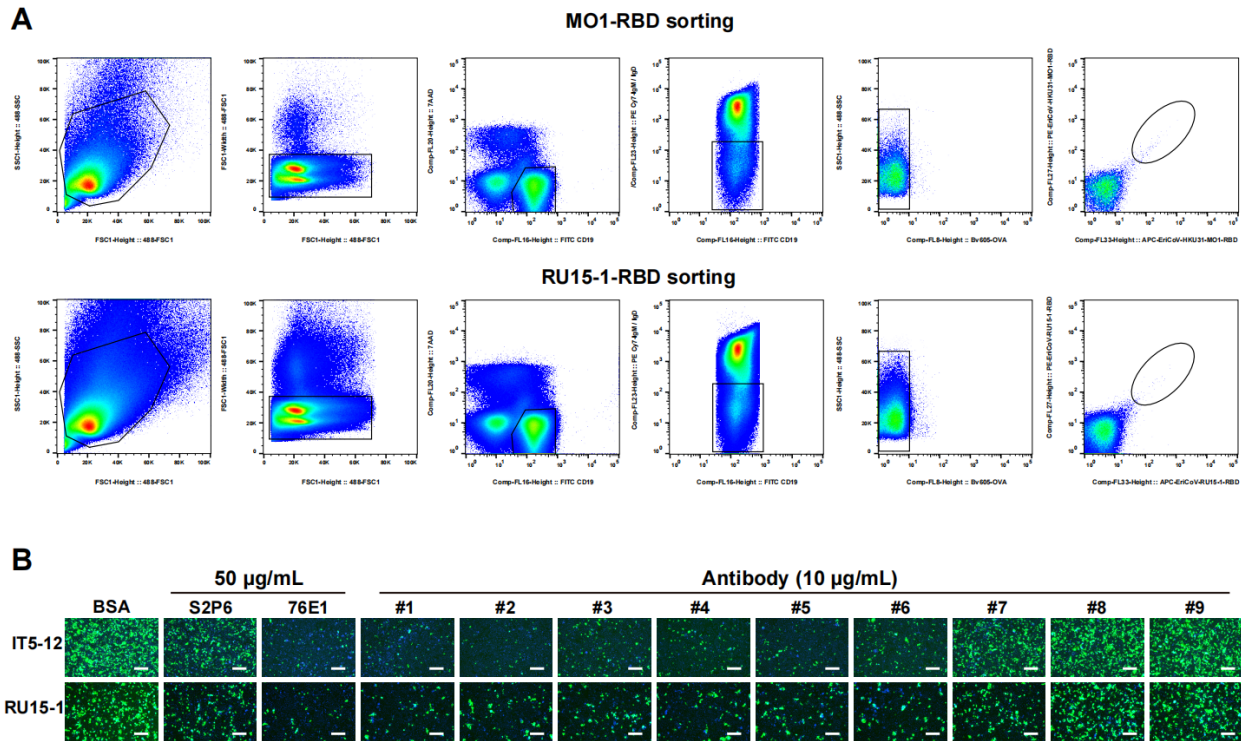


**Figure S6 | EriCoV RBD-specific antibodies efficiently inhibited the amplification of replication-competent VSV-EriCoV-S recombinant viruses.** (A) Flow cytometry gating strategy for isolation of antigen-specific B cells. Splenic B cells were pooled from immunized BALB/c mice and stained for surface markers and antigen probes. The gating strategy is shown for two representative samples: MO1-RBD (top) and RU15-1-RBD (bottom). Lymphocytes were first identified based on FSC and SSC profiles, followed by doublet exclusion. Live cells were gated by excluding 7-AAD<sup>+</sup> events. CD19<sup>+</sup> B cells were selected, and IgM<sup>-</sup>/IgD<sup>-</sup> class-switched B cells were further enriched. OVA-negative (BV605<sup>-</sup>) cells were gated to exclude non-specific binding. Antigen-specific B cells were identified as double-positive for PE-conjugated SA-MO1-RBD or SA-RU15-1-RBD and APC-conjugated SA-MO1-RBD or SA-RU15-1-RBD, respectively. These antigen-binding B cells were subsequently sorted for downstream single-cell V(D)J sequencing and antibody cloning. (B) Inhibition of rcVSV-EriCoV-S propagation by neutralizing antibodies using Caco-2 cells stably expressing the *E.amu* APN. IC<sub>50</sub> values from single-round pseudovirus assays are shown above each panel. BSA: Bovine serum albumin, 10 µg/mL. Scale bars: 200 µm.

**Table S1** Cryo-EM data collection and atomic models refinement statistics

**Table S2** Sequence information of 121 EriCoV-specific antibody sequences

**Table S3** Demographic data for the plasma donors